INVESTIGATING THE EFFICACY OF NON-IONIC SURFACTANTS AS COMPATIBILIZING AGENTS FOR POLYETHYLENE-POLYAMIDE SINTERED POLYMER BLENDS

INVESTIGATING THE EFFICACY OF NON-IONIC SURFACTANTS AS COMPATIBILIZING AGENTS FOR POLYETHYLENE-POLYAMIDE SINTERED POLYMER BLENDS

By: MOHAMMAD AKHTAR, B.Eng.

A Thesis Submitted to the School of Graduate Studies in Partial Fulfillment of the Requirements for the Degree of Master of Applied Science

McMaster University

MASTER OF APPLIED SCIENCE (2021) McMaster University

(Department of Chemical Engineering) Hamilton, Ontario

TITLE:	Non-Ionic Surfactant Stabilised Polyethylene-Polyamide Polymer Blends
AUTHOR:	Mohammad Akhtar, B.Eng. (McMaster University)
SUPERVISORS:	Professor Dr. Michael R. Thompson, Professor Emeritus Dr. John Vlachopoulos
NUMBER OF PAGES:	xv, 94

Lay Abstract

This thesis investigates the effects of non-ionic surfactants and mixing strategies on stabilising immiscible $HDPE$-$PA11$ rotomolded physical blends; surfactants were chosen over polymeric compatibilizers since the latter could not be well mixed to cover all surfaces of the two polymers both economically and safely. The physical blends were dry-mixed directly inside the rotomolding mold, whereas the extrusion-mixed blends were first mechanically compounded before being rotomolded. Densities for both, dry- and extrusion-mixed blends improved with the incorporation of Tween 20. The surfactant enhanced the impact strength of dry-mixed blends whereas it had the opposite, adverse effect in extrusion-mixed blends. Conversely, Tween 20 improved the flexural strength of extrusion-mixed blends and decreased it in dry-mixed blends. Tween 20 facilitated a mild degree of polymer migration in 50/50 dry-mixed blends, whereas the observations for 75/25 blends were inconclusive. Lastly, the presence of Tween 20 introduced increased undesirable voidage in both 50/50 and 75/25 extrusion-mixed samples.

Abstract

A novel strategy was considered in this work to improve the physical properties of rotationally molded parts formed using a thermodynamically immiscible physical blend of high-density polyethylene ($HDPE$) and polyamide 11 ($PA11$). Morphology of the melted system of the two polymers dry-mixed in the mold was dictated by the selected non-ionic surface-active agents. Through a preliminary evaluation of numerous non-ionic surfactants, Span 85 and Tween 20 showed the most promise at concentrations between 0.1 - 1.0 wt% for influencing how the two polymers spread over the mold surface in a uniaxial rotational molding unit; the two surfactants demonstrated favourable interparticle cohesion at 235 °C and were chosen on the basis of investigating the hydrophilic-lipophilic balance (HLB) as a predictive metric for polymer migration during rotomolding. For a comparison to a more traditional (and expensive) approach of preparing a molded part with blends of these two polymers, extrusion-mixed blends were first compounded using a twin-screw extruder, pelletized, ground, and finally rotomolded.

The good compatibility of the two constituent polymers with Tween 20 was demonstrated by decreasing zero-shear viscosities with increasing surfactant concentration. In the molded samples, porosity for 50/50 dry-mixed blends increased at low concentrations of Tween 20, but ultimately the surfactant demonstrated its beneficial nature on sintering with a downward trend observed in porosity with increasing surfactant concentration; molded samples with 1.0 wt%

Tween 20 showed a 1% improvement in porosity relative to uncoated blends, whereas 1.0 wt% Span 85 coated blends showed an undesirable increase in porosity instead. Similar trends were observed for 75/25 dry-mixed blends, except that the porosities for all Tween 20 concentrations were lower than those of uncoated blends. Low porosities were observed for all extrusion-mixed blends (with or without 1.0 wt% Tween 20) relative to the dry-mixed blends. As more favourable results for this new approach, Tween 20 coated dry-mixed blends showed an increase in impact strengths for both blend ratios, whereas extrusion-mixed blends showed a drastic decrease instead. Conversely, the inverse trend was found with flexural strengths. The results were reconciled through morphological analysis of the molded samples which demonstrated that a moderate degree of polymer migration occurred (i.e. aggregation of $PA11$ at the wall boundaries and $HDPE$ near the centre) in the presence of the surfactant for 50/50 dry-mixed blends, whereas observations for the 75/25 blends were inconclusive. Therefore, based on the observations for density/porosity, impact strength, flexural strength, and morphology (i.e. polymer migration) modifying the blend-ratio, mixing strategy, and surfactant concentration for rotomolded $HDPE$-$PA11$ physical blends enables us to reliably predict and control the polyblends' resultant properties and cater them to meet the requirements of a wide range of unique and specific use-case scenarios.

Acknowledgements

I would like to express my sincerest gratitude to my supervisor, Dr. Michael Thompson for his unyielding confidence, patience, and guidance over the course of my graduate studies. Undoubtedly, without his invaluable mentorship, this thesis would not be possible. I would also like to thank my co-supervisor Dr. John Vlachopoulos, and Ron Cooke for their constructive feedback and insight along the way. Additionally, I would like to extend my heartfelt appreciation to Dr. Charles de Lannoy, Dr. Jake Nease, Dr. Boyang Zhang, Dr. Todd Hoare, Heera Marway and the rest of my colleagues in the Michael Thompson Research Group, and the Department of Chemical Engineering for their continuous support during my time as both, an undergraduate and graduate student at McMaster University. I would also like to thank Imperial Oil Ltd. and the Natural Sciences and Engineering Research Council for their continuous support, fiscally and otherwise. Last but most certainly not least, I am eternally indebted to the support, encouragement, and prayers of my family. Amongst whom, the women in my life have served as the greatest inspiration and motivation for my efforts and success in both, my personal and professional life.

Table of Contents

List of Figures

List of Tables

List of Abbreviations and Symbols

$ASTM$	American Society for Testing and Materials
ATR	Attenuated total reflectance
c	FBR spray coating correction factor
CM	Compression molding
DSC	Differential scanning calorimetry
E_s	Specimen breaking energy
E_{TC}	Total correction energy for E_s
$EVOH$	Ethylene-vinyl alcohol
f	Porosity
FBR	Fluidized bed reactor
$FT\text{-}IR$	Fourier-transform infrared spectrometry
h	Height
$HDPE$	High density polyethylene
HLB	Hydrophilic-lipophilic balance
I_s	Impact strength
I_s^*	Specific impact strength
$LLDPE$	Linear low-density polyethylene
$LLDPE^*$	Modified linear low-density polyethylene
$\dot{m}_{FBR}$	FBR spray mass flow rate
m_{p_i}	Mass of constituent polymer, i

m_s	Mass of surfactant, s
$PA11$	Polyamide 11
PFT	Plastic fuel tanks
$PIAT$	URM peak internal air temperature
R	Rate of crosshead motion
$\dot{r}_{DSC}$	DSC heating and cooling ramp rate
$\dot{\bar{r}}_{C\|URM}$	URM average cooling rate
S_{85}	Span® 85, sorbitan trioleate
SMD	Sauter mean diameter
S_e	External surface of rotomolded cuboid
S_i	Internal surface of rotomolded cuboid
T_{20}	Polysorbate 20, Tween® 20, polyoxyethylene sorbitan monolaurate, PEG sorbitan monolaurate
T_c	Crystallisation temperature
t_{FBR}	FBR spray coating time/duration
T_m	Melting temperature
$T_{SP\|URM}$	URM oven platens set-point temperature
TSE	Twin-screw extruder/extrusion
T_{VAC}	Vacuum oven temperature
URM	Uniaxial rotomolding or rotational molding
v	Volume

w_{p_i}	Constituent polymer mass fraction (i.e. $HDPE$ or $PA11$)
w_s	Surfactant mass fraction (i.e. T_{20} or S_{85})
$w_{T_{20}\|TSE}$	Mass fraction of T_{20} coated $HDPE$ particles via FBR for TSE
ΔG_m	Change in Gibbs free energy at melting temperature
ΔH_c	Change in enthalpy at crystallisation temperature
ΔH_m	Change in enthalpy at melting temperature
ΔS_m	Change in entropy at melting temperature
η_0	Zero-shear viscosity
η_C	Cross model viscosity
η_{CY}	Carreau-Yasuda viscosity
$[\eta]$	Intrinsic viscosity
ϑ	FBR nozzle spray angle
ρ_{CM}	Compression molded neat polymer density
ρ_i	Density of component, i
ρ_{URM}	Rotomolded blend density
σ_f	Flexural stress
σ_f^*	Specific flexural stress
φ	Void fraction
$\emptyset$	Diameter

Declaration of Academic Achievements

The majority of the work presented in this thesis was completed and written by the author in consultation and with editorial assistance from supervisors, Dr. Michael R. Thompson and Dr. John Vlachopoulos. This thesis contains no material that has been submitted previously, in whole or in part, for the award of any other academic degree or diploma.

Chapter 1. Introduction

Semi-crystalline thermoplastics are a subcategory of synthetic polymers, which when heated above their melting point T_m, can be purposefully shaped through the use of specialised dies or molds via polymer processing technologies such as extrusion and rotational molding. The molten thermoplastic is subsequently solidified by cooling below its crystallisation temperature, T_c [1], thereby fixing its shape permanently (disregarding recycling and degradation). Encompassing a diverse range of distinct material properties, this class of polymers may be blended, reinforced, or compounded to produce "value-added" finished products [2]. Constituent components of a polymer blend are selected on the basis of each component's inherent properties, ideally complementing the utility of the other, while mitigating adverse interactions [3]. Intrinsic properties of otherwise incompatible polymers render blends thereof immiscible and susceptible to phenomenologically poor dispersion morphology and weak interfacial adhesion [4]. Physical or chemical compatibilization is used to overcome immiscibility primarily through the reduction of interfacial tension and suppression of droplet coalescence [5, 6]. Research and development of novel multiphase polymer blends is primarily incentivised by the economic viability, competitive advantage, and specific functionality it provides in a particular application or end-user scenario. The application of interest for this study is a fuel-impermeable plastic storage tank made by rotational molding methods.

Today, Plastic Fuel Tanks ($PFTs$) comprise approximately 90% of all fuel tanks manufactured in Europe and 75% of automotive fuel tanks in the United

States, with high-density polyethylene ($HDPE$) as the preferred polymer of choice [7]. Compared to traditional steel fuel tanks, $PFTs$ do not require corrosion inhibitors, are characteristically less dense (i.e. lightweight), and provide better processability, formability, durability, and recyclability [8]. Additionally, $PFTs$ have proven to be considerably safer than metallic fuel tanks in cases of emergencies or in the event of an accident [9]. Despite its versatility however, non-polar $HDPE$ is highly susceptible to fuel permeation and evaporative emissions. $HDPE$ is commonly formed by chain addition reactions of ethylene monomers via coordination polymerisation resulting in tightly packed linear hydrocarbon chains as shown in Figure 1.1.

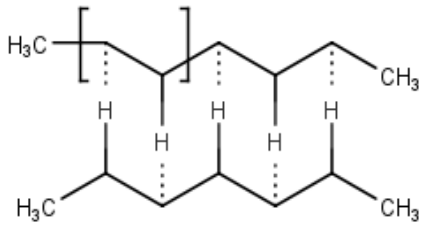

Figure 1.1. Hydrogen-carbon Van der Waals interactions in high-density polyethylene; repeating unit designated by square brackets.

The short aliphatic and aromatic chains of gasoline can permeate through the long macromolecular chains of $HDPE$, whereas the percolation of diesel is largely stymied due to its longer hydrocarbon chains [8]. To circumvent this issue, a variety of barrier technologies are used, such as fluorination of the internal surface of a $HDPE$ fuel tank or embedding low-permeability polymers such as ethylene-vinyl alcohol ($EVOH$) or polyamides (PA) between layers of $HDPE$ via co-extrusion and

blow-molding processes [8, 10]. The latter case scenario requires polar-functionalised polyolefin adhesive resin to bind the otherwise incompatible $HDPE$ and low-permeability polymer layers, such as maleic anhydride modified linear low-density polyethylene ($LLDPE^*$) [11]. Alternatively, $HDPE$ and polar polymers with favourable barrier properties may be compatibilized using block or graft copolymers or polymeric solvents [2].

The conventional method employs blow-molding to manufacture a five-, seven-, or nine-layer impermeable tank. The process may generate upwards of 40% scrap (i.e. flash and defective parts). This material can be reground and used as an 'off-spec' core layer in the tank [8]. Therefore, this process requires a combination of complex extrusion and blow-molding technologies to produce an impermeable PFT.

The challenges of processing zero-emission tanks based on immiscible polymer blends become exaggerated as the tank sizes are upscaled to accommodate larger vehicles, such as marine vessels, agricultural machinery, and even commercial trucks. Where the additional costs associated with manufacturing larger fuel tanks are unmerited using blow-molding methods, rotational molding is often preferred. However, literature and research on blending resins is scarce, especially where one phase is required to act as a barrier to penetrants.

Rotational molding is the ideal thermoplastic processing technique to manufacture large, hollow plastic parts. Contrasting the complexity and fiscal overhead of co-extrusion and blow-molding processes, rotomolding is a relatively

simple, inexpensive, zero-shear technique which produces seamless plastic parts of complex geometries and low residual stresses. Not unlike conventional small-scale automotive $PFTs$, rotomolded $PFTs$ are required to be both structurally sound and fuel-impermeable. For instance, in order to manufacture a multi-layered $HDPE$-based rotomolded PFT, the polyethylene is first crosslinked to permanently hold its shape before the higher melting temperature polar resin is cast inside to add barrier properties. Alternatively, linear low density polyethylene ($LLDPE$) may also be used for the outside layer of a rotomolded PFT, though such a structure is more complex to process. The combination of immiscible non-polar $HDPE$ and polar $PA11$ (shown in Figure 1.2) as constituent structural and impermeable polymers, respectively, in PFT solutions is not entirely without precedent [12].

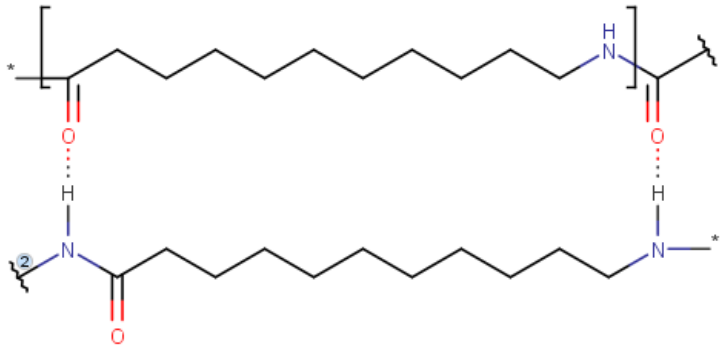

Figure 1.2. Hydrogen-oxygen hydrogen bonding in polyamide 11; repeating unit designated by square brackets.

Compared to the industry standards for manufacturing $HDPE$-PA $PFTs$ discussed above, a proposed physical blend method for rotational molding has two distinct advantages: *simplicity* and *economy*. The production of multi-layered

structures requires specialised equipment and introduce complexity to the process [13]. For the physical blend method to succeed though, the two polymer phases must be encouraged to spread over one another in a controlled manner, which implies a need for surface active agents to be included with $HDPE$ and $PA11$.

Compatibilizers or surfactants can stabilise and direct the morphology of rotomolded immiscible blends. Compatibilizers have high viscosities, benefiting the interfacial energy of these immiscible blends via chain entanglement for domain adhesion, and surface-active functionality in both phases. Conversely, surfactants are lower viscosity, smaller molecular species that may only lower the interfacial tension between dispersed phases but should demonstrate faster diffusion to these interfaces compared to a compatibilizer. For rotomolding, surfactants will be superior to compatibilizers, if being directly added to the process rather than compounded into the resins, since diffusion control will minimize good distribution of highly viscous surface-active species to all particle-particle interfaces during sintering. Therefore, an investigation into surfactant suitability for stabilising immiscible polymer blends is alluring, both in terms of its economic viability and immediate adoptability by industry.

The purpose of this project was to investigate the efficacy of non-ionic, amphiphilic surfactants, polyoxyethylene sorbitan monolaurate (Tween 20) and sorbitan trioleate (Span 85), as compatibilizing agents for stabilizing a physical blend of semi-crystalline polymers, specifically high-density polyethylene ($HDPE$)

and polyamide 11 ($PA11$) in a rotational molding process to prepare fuel tanks; the proposed interactions of $PA11$ and $HDPE$ with Tween 20 are shown in Figure 1.3.

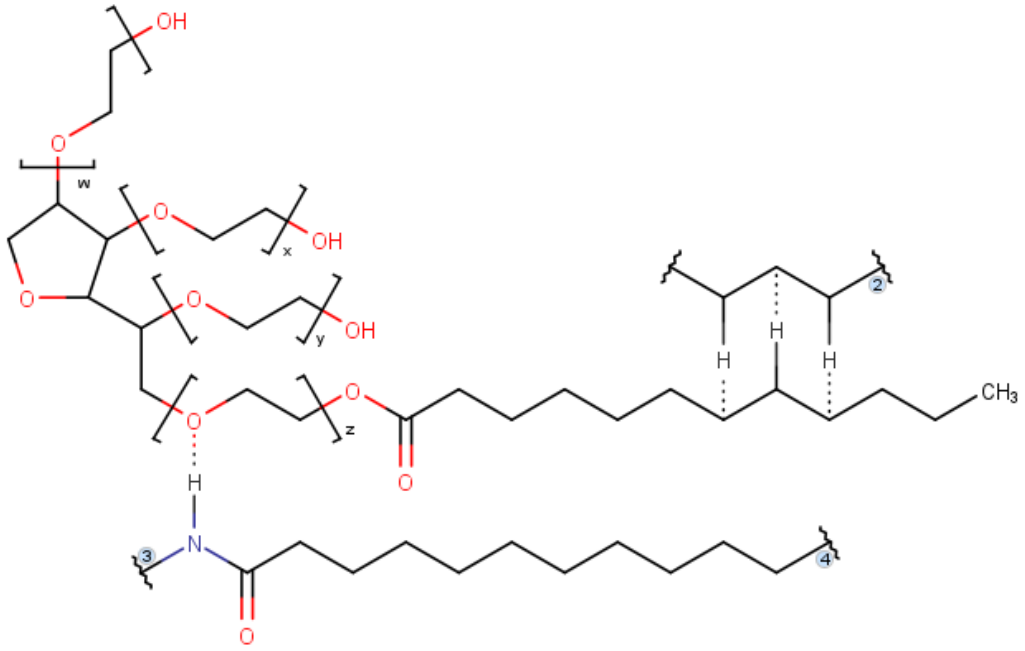

Figure 1.3. Hydrogen-bonding with polyamide 11 and dipole-dipole bonding in high-density polyethylene, with the hydrophilic head and the hydrophobic tail of polyoxyethylene (20) sorbitan monolaurate (i.e. Tween 20), respectively.

The research objectives were:

- Propose a method as a single-step process wherein $HDPE$ and $PA11$ polymer resins, approximately 500 μm in Sauter mean diameter (SMD), are sintered as a dry-mix blend via rotational molding to produce a part with improved impact strength and resistance to fuel emissions and permeability. The study considers the influence of increasing surfactant concentration on part performance.

- Compare the proposed method to a case where the surfactant was pre-mixed into the polymer via twin-screw extrusion, and then rotomolded. The durability of the rotomolded parts produced via both methods was analysed through mechanical testing and a detailed examination of the sintering quality.

This thesis includes a concise review of the fundamental concepts relevant to the topic, in particular, the principles of thermoplastic rotomolding, interfacial adhesion, interdiffusion, miscibility, and the functionality of compatibilizing agents, as presented in *Chapter 2*. An explicitly detailed and comprehensive overview of the materials used, and experimental techniques employed to interpret the results and test the hypotheses presented herein, is covered in *Chapter 3*. The aforementioned experimental characterisations of rotomolded blends, accompanied by an in-depth discussion of the results, validated, and supported by comparable results elsewhere in literature are presented in *Chapter 4*, followed by a succinct conclusion of the results and recommendations for future work in *Chapter 5*.

1.1 References

[1] M. Jafar Mazumder, H. Sheardown and A. Al-Ahmed, *Functional Polymers*. Cham: Springer International Publishing, 2020.

[2] L. Utracki, *Polymer alloys and blends*. Munich: Hanser, 1990.

[3] N. Cheremisinoff, *Handbook of engineering polymeric materials*. New York: M. Dekker, 1997.

[4] M. Chanda and S. Roy, *Plastics Technology Handbook, Fourth Edition*. Hoboken: CRC Press, 2006.

[5] D. Paul and S. Newman, *Polymer blends*. New York: Academic Press, 1978.

[6] U. Sundararaj and C. Macosko, "Drop Breakup and Coalescence in Polymer Blends: The Effects of Concentration and Compatibilization," *Macromolecules*, vol. 28, no. 8, pp. 2647-2657, 1995. Available: 10.1021/ma00112a009.

[7] L. Shafigullin, A. Sotnikov, N. Romanova, E. Shabaeva and D. Sarimov, "Development of a polymeric fuel tank with high barrier properties," *IOP Conference Series: Materials Science and Engineering*, vol. 570, p. 012088, 2019. Available: 10.1088/1757-899x/570/1/012088.

[8] P. Delbarre and A. Rodi, "Barrier Technologies Applied to Plastic Fuel Tanks: Comparison of Their Performance," *SAE Technical Paper Series*, 1999. Available: 10.4271/1999-01-3029.

[9] T. Ellis, J. Laverty and M. Lesinski, "Recyclability and Characterization of Co-Extruded Multilayer Fuel Tanks," *SAE Technical Paper Series*, 1998. Available: 10.4271/980096.

[10] Z. Benrabah, F. Thibault and R. DiRaddo, "Modeling of Fuel Permeation in Multilayer Automotive Plastic Fuel Tanks," *SAE International Journal of Materials and Manufacturing*, vol. 4, no. 1, pp. 449-459, 2011. Available: 10.4271/2011-01-0248.

[11] I. Abu-Isa, S. Khalid, G. DeBarr and S. Zhi, “Mechanical, Thermal and Rheological Properties of Polymers Used in Plastic Fuel Tanks,” *SAE Technical Paper Series*, 2006. Available: 10.4271/2006-01-0333.

[12] K. Fukuhara, M. Hara, N. Matsuura and H. Watanabe, “Development of Plastic Fuel Tank Using Modified Multi-Layer Blow Molding,” *SAE Technical Paper Series*, 1990. Available: 10.4271/900636.

[13] E. Jansri and N. O-Charoen, “Polypropylene/polyethylene two-layered by one-step rotational molding,” *Journal of Polymer Engineering*, vol. 38, no. 7, pp. 685-694, 2018. Available: 10.1515/polyeng-2017-0367.

Chapter 2. Literature Review

2.1 Principles of Thermoplastic Rotomolding

2.1.1 Introduction

Essentially a four-step process, rotomolding begins with loading polymer resin into a mold cavity, designed in the form of a negative impression of the desired product. After the initial step, also known as charging, the mold is simultaneously rotated uniaxially or biaxially and heated to the desired temperature [1], commonly referred to as the peak internal air temperature or $PIAT$. Thereafter, the mold is subsequently cooled to below the resin's crystallisation temperature, T_c (assuming semi-crystalline polymer(s) is used). If the resin is comprised of a blend of two or more polymers, the mold is cooled below the crystallisation point of the constituent polymer with the lowest T_c. Upon solidification, the hollow plastic part is retrieved having taken the shape of the reverse impression of the mold cavity (i.e. positive impression of the desired product).

$PIAT$ is ideally measured at the approximate centroid (i.e. geometric center) of the mold in the rotomolding apparatus as described in § 3.2.3, corresponding to the cooler end of the temperature gradient normal to the mold wall, which exists across the molten polymer resin. The onset of the cooling cycle triggers the densification of the molten polymer into a unified layer starting at the mold wall [2]. Temperature management within the mold and consequently the material properties of rotomolded samples are governed by an acute understanding and control over the radiative and convective heat transfer mechanisms, which exist

between the heating (i.e. electric, microwave) and cooling (air, atomized water) elements, the enclosed mold surface, and the polymer resin within [3]–[5].

Compared to alternative polymer processing techniques such as co-extrusion and blow-molding, rotational molding produces geometrically complex single- or double-walled parts in a near zero-shear environment resulting in negligible residual stresses [1]. The uniaxial or biaxial rotation in rotomolding is relatively slow, normally ranging between 4 - 20 RPM. Therefore, any resultant centrifugal forces generated play a negligible role in a rotomolding process and melt flow behaviour is predominantly driven by the development of slip flow regimes [6], [7]. Owing to its simplicity and adaptability, it is not uncommon for industries specialising in the manufacturing of relatively large and structurally demanding components such as those commonly found in boats and wind turbines, to adopt rotational molding as their polymer processing method of choice [8].

2.1.2 Process Control Variables

Rotomolding heating elements do not function as an adiabatic system, and therefore, temperature within the mold during the heating and cooling cycles cannot be treated as a function of an isothermal environment. Consequently, the inhomogeneous heating and cooling render process control particularly difficult [9]. In addition, poor surface topography and relatively long cycle times constitute some of the key drawbacks of polymer processing via rotomolding methods [1]. Undesirable surface defects and deformations are in large part due to the thermal instability of polymers and non-ideal $PIAT$s. As a result, variants of high-density

polyethylene such as $HDPE\ HD\ 8660.29$ (Imperial Oil Ltd.) and other common rotomolding resins are often stabilized to improve their thermal performance when exposed to elevated temperatures for prolonged periods of time. Regardless, carefully selecting the $PIAT$ is nonetheless crucial, given that in a zero-shear processing environment, which is otherwise advantageous as mentioned earlier, the most critical parameter for controlling the final characteristics of a rotomolded part is temperature. Low $PIAT$ may result in poor particle cohesion and increased surface porosity, whereas high $PIAT$ may cause thermo-oxidative degradation [10]. Similarly, the rate at which the molten resin is subsequently cooled may result in deformation and warpage during densification [11].

Beyond aesthetics, high surface porosity and bubble formation in rotomolded elements suggest poor mechanical, tensile, and permeability properties. As such, considerable time and effort has been dedicated to developing models that can effectively predict the sintering behaviour responsible for the aforementioned material defects. The mechanism of bubble formation via sintering is understood to describe the entrapment of air during the fusion and consolidation of molten polymer particles and subsequent decrease in total surface area due to surface tension [12]. To that end, despite its limitations, the Frenkel-Eshelby model has served as the foundation for describing sintering behaviour in both glass and polymeric materials [13]–[18]:

$$\frac{x}{r} = \left(\frac{t\gamma}{\mu r_0}\right)^{\frac{1}{2}} \tag{2.1}$$

where, x, r, and r_0 are the neck, sphere, and initial particle radii, respectively, γ is the surface tension, μ is viscosity, and t is time.

The schematic in Figure 3.2 visualises the Frenkel-Eshelby model for neck growth kinetics (left-to-right), where two adjacent particles, when exposed to heat via hot-stage microscopy, lead to the development of neck formation along the grain boundaries due to diffusion, ultimately resulting in the coalescence (i.e. bonding) of both particles.

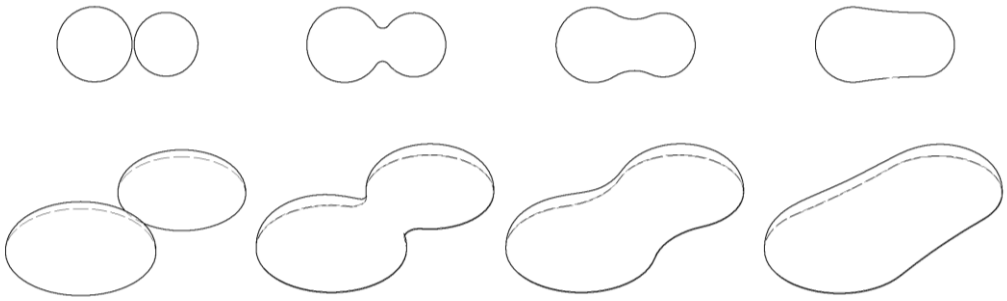

Figure 2.1. Particle-particle coalescence in zero-shear sintering environments.

In addition to viscosity and surface tension, polymer resin characteristics such as particle shape and size distribution, packing density, particle cohesion and coalescence, and slip-flow regimes have been shown to directly impact thermal conductivity, mixing, tortuosity, and void fraction [19]–[23]. Therefore, a careful balance must be achieved between the various control variables to achieve proper mixing, efficient heat transfer, low porosity, high packing density, and low inter-particle space during sintering. Furthermore, achieving a delicate balance between $PIAT$, cycle time, melt-flow index (MFI), viscosity, and compatibilizer

concentration can result in greater interfacial adhesion and lower surface tension, therefore yielding a decrease in bubble formation and voidage [12], [24].

However, this balance must be offset to account for any loss of desirable material properties due to thermo-oxidative polymer degradation [10, 25]. For instance, although an increase in $PIAT$ has been shown to effectively collapse and decrease bubble formation [12], the dramatic deterioration of mechanical properties in rotomolded elements, due to prolonged exposure to elevated temperatures [26], may necessitate accepting some degree of deformation and voidage to meet other, more application-relevant product specifications. As such, the ideal $PIAT$ is conventionally selected to be just below the onset of thermal instability of the constituent polymer resins [27], [28]. If a higher $PIAT$ is necessary however, heat stabilizers can be introduced into the system to inhibit thermal degradation [25].

Not unlike heating during melting, cooling, or more specifically, cooling rates during densification can influence the quality of rotomolded elements as well. As the molten polymer resin cools, a temperature and a crystallinity gradient develop across the melt due to the outermost layer (i.e. contacting the mold surface, exposed to the cooling elements) cooling more rapidly than the innermost layer (i.e. the free surface). As such, the temperature gradient results in the onset of a stress profile and consequently, a bending moment to compensate for said stresses, which can lead to warpage and residual stresses in the final unified layer of the rotomolded part [29]–[31].

Similarly, crystallisation affects the morphology across the cross-sectional profile of the rotomolded elements due to the imbalance between nucleation and the development of coarse and fine spherulites between the inner and outermost layer, respectively [32], [33]. In semi-crystalline polymer blends, innate characteristics of the constituent components have been shown to elicit substantial deviations from the normal nucleating activity, spherulite growth rate, and crystallisation behaviour of each polymer due to the presence of the other [34]. In heterogeneous polymer blends, co-crystallisation kinetics are governed by the primary nucleation step, where the crystallisation of the continuous phase in the presence of a molten or solidified dispersed phase, and vice-versa, can affect the nucleating activity of each component and the migration of heterogeneities at the interphase [35]. Furthermore, the degree to which the coincident or sequential crystallisation of the dispersed and continuous phases effects the morphology of a semi-crystalline polyblend, is also dependent on the blend composition. In some scenarios, this means that the relative crystallisation behaviours of the constituent components, normally at low concentrations of the dispersed phase, have a negligible effect on the thermal behaviour and morphological development of the blend system [36]. Nonetheless, temperature control (or lack thereof) in a rotomolding process can further exacerbate the effects of crystallisation behaviour in heterogeneous polyblends on the resultant mechanical properties of a rotomolded blend.

The optimisation of the process control parameters and variables, including but not limited to temperature, composition, and compatibilization strategies is achieved via the evaluation of the resultant material properties of rotomolded polyblends. To that end, both low- and high-speed material characterisation techniques are used to evaluate a rotomolded blend's performance against its designated or intended use-case scenario. Low-speed material characterisation techniques evaluate a polymer blend's tensile strength, tensile modulus, flexural strength, etc. whereas high-speed characterisation methods test properties such as impact strength, crack-resistance, fracture mechanics, etc. [37].

2.2 Thermoplastic Polymer Blends

2.2.1 Common Commodity and Engineering Resins

The materials industry's transition from single-phase commodity (e.g. polyethylene, polypropylene, etc.) and engineering (e.g. polyamides, polyesters, etc.) polymers to value-added multi-phase polymeric blends has catalysed the research and innovation of novel polymerisation methods, processing techniques, and compatibilizing/reinforcing mechanisms. Commodity polymers constitute approximately 79% of the market share of total synthetic polymer production [38], of which polyolefins in particular and blends thereof account for more than 33% [39]. Furthermore, polyethylene accounts for approximately 90% of all resins commonly used to produce rotomolded parts [2]. This includes, all varieties and grades of polyethylene ranging from very-low-density polyethylene ($VLDPE$) to ultra-high-molecular-weight polyethylene ($UHMWPE$); each with distinctly

unique properties based on variations in molecular weight, molecular weight distribution, and branching [40].

Notwithstanding its general immiscibility in nearly all multi-phase blends, polyethylene is often blended with elastomers and polypropylene to improve its impact strength and flexural properties; intermixed with different grades of polyethylene to aid processability and improve mechanical performance; and with polyamides to improve its mechanical properties, absorptivity, rigidity, and barrier properties [38]. Similarly, polyamide has been shown to improve its processability, solvent resistance, mechanical properties, and even its otherwise notable barrier properties with the addition of other synthetic polymers and/or intermixing of other polyamide grades. These grades are commonly represented as PA, suffixed with the number of carbons present in the diamine and carboxylic acid groups of a single monomer chain (e.g. $PA6$, $PA6{,}6$, $PA11$, and $PA12$).

2.2.2 Biphasic Blend Morphology

As per Utracki [38], standardised nomenclature defines a polymer blend in which the constituent components comprise at least 2 wt%. Compared to economically intensive novel polymerisations or polymer syntheses, which require exhaustive research and development, polymer blending processes yield new polymeric materials by utilising the diversity and utility of existing polymers with a combination of each's uniquely distinct and otherwise conflicting properties. The intermingling of polymer properties and the phase dispersion morphology in biphasic blends can be characterised in terms of the concentration of its constituent

components, wherein the dispersed phase and continuous matrix describe the low- and high-concentration components, respectively. At low concentrations, the dispersed phase forms spherical droplets within the continuous matrix. As the concentration of the minor component increases, the dispersed phase forms regions of continuity, with the blend reaching full co-continuity at the phase inversion concentration point, where the dispersed and the continuous phase are virtually indistinguishable. This variation in phase dispersion morphology or phase separation due to nucleation growth or spinodal decomposition [37] is shown in Figure 2.2, where going from left-to-right, the concentration of the dispersed (i.e. white) and the continuous (i.e. shaded) phases increase and decrease, respectively.

Figure 2.2. Morphological development of the dispersed phase and continuous matrix in binary low-affinity immiscible polymer blends.

The morphological character of the dispersed phase within the continuous matrix can be correlated to the rate at which the spherical droplet diameter increases or decreases due to the dispersion and coalescence mechanisms, respectively [41]. As such, the dispersion mechanism can be explained by the following correlation:

$$\frac{\partial d}{\partial t} = -k_1 \dot{\gamma} d \tag{2.2}$$

where d is the droplet diameter, t is time, $\dot{\gamma}$ is the deformation rate, and k_1 is the dispersion proportionality constant. The coalescence mechanism is given by:

$$\frac{\partial d}{\partial t} = \frac{k_2 \dot{\gamma} \phi^{\frac{8}{3}}}{d} \tag{2.3}$$

where ϕ is the volume fraction of the dispersed phase and k_2 is the coalescence proportionality constant.

In addition to concentration, the biphasic morphological distribution, phase equilibria, the stability of its constituent components, and resultant properties are dependent on the compatibilization mechanisms employed, viscosity of blend components, and flow characteristics (i.e. mechanical compounding, fibrillation, coalescence, encapsulation, etc. [42]–[44]) of the polymer process system. Moreover, viscosity-induced flow behaviour has been shown to elicit migratory behaviour in extrusion processes, wherein the low-viscosity polymer migrates to the high-stress regions of the extrudate leading to the encapsulation of the high-viscosity resin [45]. Similarly, flow behaviour can also be influenced by the intermolecular interactions and the degree of entanglement of the blend components [46], [47].

2.2.3 Thermodynamic Immiscibility

It is exceptionally rare for polymeric materials to organically form miscible, homogenous multi-phase polymer blends. Therefore, unless aided by physical or chemical compatibilization mechanisms, polymer blends exhibit strong

immiscibility, which is characterized by poor interfacial adhesion and unstable morphological development [48], [49].

Thermodynamically macromolecular miscible polymer blends are characterised by a negative change in the free energy of mixing (ΔG_m) defined as,

$$\Delta G_m = \Delta H_m - T\Delta S_m < 0 \tag{2.4}$$

where ΔH_m and ΔS_m are the enthalpy and entropy of mixing, respectively at temperature, T. In multiphasic polymer systems, the entropy of the system is always positive due to mixing, there $T\Delta S_m > 0$, therefore miscibility as predicted by the entropy of mixing, ΔG_m can be determined by the value for the enthalpy of mixing of a binary polymer blend, which is defined by,

$$\Delta H_m = H_m - \sum x_i H_i = x_A(H_m - H_A) + x_B(H_m - H_B) \tag{2.5}$$

where ΔH_m is the enthalpy of the polymer blend, A/B, x_i and H_i are the molar fraction and enthalpy of component, i, respectively. As such, negative values for ΔH_m represent exothermic, thermodynamically miscible blends, whereas immiscible polymer blends are typically endothermic mixtures, characterised by a positive change in the enthalpy of mixing, where $\Delta H_m > 0$ [39].

2.2.4 Compatibilization

Immiscibility in multiphasic polymer blends can also be characterised in terms of the properties of the interphase. In binary heterogeneous mixtures, this

phase is a third phase, which exists between the dispersed phase and the continuous matrix. The thickness of the interphase is inversely proportional to the interfacial tension coefficient. Therefore, to reduce the immiscibility of low-affinity polymer blends, the thickness of the interphase must approach zero as the interfacial tension coefficient goes to infinity [41].

As mentioned earlier, unlike co-extrusion and blow-molded blends, rotomolded parts are physically blended in the absence of external energy input. Therefore, compatibilizers or surfactants must be utilized to stabilise immiscible blend phase dispersion morphology. To that end, processing methods for multi-phase polymeric materials typically incorporate mechanical and/or compatibilization techniques to overcome the immiscibility of synthetic semi-crystalline thermoplastics. Compatibilizers achieve this by optimizing for the thermodynamic equilibrium between the dispersed phase and the continuous matrix [41].

Compatibilization strategies for biphasic blends include the addition of an aliphatic copolymer to the blend, miscible with both constituent components (as shown in Figure 2.3 for a $HDPE\text{-}PA11$ blend), the development of localised miscibility via reactive compounding, and stabilising morphology using nanoparticles. Compatibilizers achieve this via entanglement, fostering domain adhesion and lowering the surface energy between the immiscible phases. Whereas surfactants, which are considerably smaller in size, may only stabilise immiscible blends by lowering the interfacial tension between the dispersed phases. Although

seemingly overwhelmingly advantageous, compatibilizers are often catered to very specific use-cases, the synthesis of which in terms of the time, money, and resources dedicated to researching and producing them is often unwarranted and unjustified.

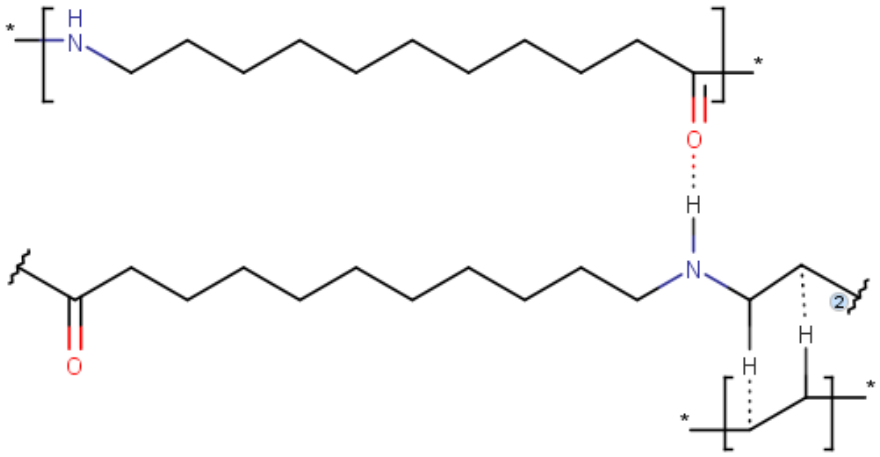

Figure 2.3. $HDPE\text{-}PA11$ block co-polymer compatibilizing agent.

Therefore, the focus of this thesis is the addition of surfactants to binary immiscible blends. Surfactants owing to their amphiphilic nature, may behave similarly to copolymers in reducing the interfacial tension between the two phases (as mentioned earlier), but they are generally expected to perform poorly in comparison to compatibilizers when it comes to improving the interfacial adhesion or stabilising morphology [38]. The hydrophilic and lipophilic regions of surfactants such as sorbitan esters and their ethoxylated variants are non-specialised, therefore their structural topography or functional groups may not be as effective as copolymers, and possibly may even hinder or worsen interfacial adhesion. Conversely, the amphiphilic character of copolymers is typically

designed to cater to the unique polar and non-polar regions of both components in a binary polymer blend.

2.3 Hydrophilic-Lipophilic Balance

Since the role of compatibilizers in polymer blends may be understood to be identical to that of emulsifiers in classical emulsions [49], surfactants such as sorbitan esters and their ethoxylated variants may prove equally as effective in stabilising immiscible polymers. This is because amphiphilic surfactants like Tween 20 have hydrophilic and lipophilic regions that can act as an adhesive and form intermolecular bonds with both $HDPE$ and $PA11$ polymer as shown in Figure 1.3.

Moreover, the hydrophilic-lipophilic balance (HLB) of surfactants, whether high or low, can approximate the stabilisation of a colloidal suspension as either an oil-in-water or water-in-oil emulsion. Although Pasquali et. al [50] have proposed alternative models to determine the HLB of surfactants, the original classification model by Griffin [51] is used herein. For non-ionic polyoxyethylene esters, HLB can be calculated using the mass percentage of oxyethylene content E, where:

$$HLB = \frac{E}{5} \tag{2.6}$$

HLB may also be determined using the saponification value of the ester, S and the acid value, A. A sample calculation for Tween 20 is given below [52]:

$$HLB = 20\left(1 - \frac{S}{A}\right) \tag{2.7}$$

$$HLB = 20\left(1 - \frac{45.5}{276}\right) = 16.7$$

The HLB of blended surfactants with known HLB values can be determined using the mass fraction, f_i and HLB_i of component i, where:

$$HLB = \sum HLB_i \times f_i \tag{2.8}$$

Theoretically, the use of Span 85 (HLB = 1.8) and Tween 20 (HLB = 16.7) as compatibilizing agents may effectively predict and elicit the melt-phase polymer migration of the constituent polymers, resulting in $PA11$-in-$HDPE$ or $HDPE$-in-$PA11$ physical blends, respectively. This is especially relevant for $50/50$ dry-mixed and $25/75$ extrusion-mixed blends (i.e. at the approximate phase-inversion concentration for $HDPE$-$PA11$ blends; see § 4.4.1). Notwithstanding the relevance of $HDPE$-in-$PA11$ in plastic fuel tank (PFT) applications, Tween 20 and some minor consideration of Span 85 surfactants are investigated herein to test the polymer-migration hypothesis.

2.4 References

[1] K. Ogila, M. Shao, W. Yang and J. Tan, "Rotational molding: A review of the models and materials," *Express Polymer Letters*, vol. 11, no. 10, pp. 778-798, 2017. Available: 10.3144/expresspolymlett.2017.75.

[2] R. Crawford and J. Throne, *Rotational Molding Technology*. Norwich, NY: William Andrew Publishing, 2002.

[3] W. Khan and J. Methven, "Control of the uniformity of direct electrical heating for Rotational Moulding," in *Proceedings of the 36th International MATADOR Conference*, London, UK, 2010. pp. 87-90.

[4] M. P. McCourt, M. P. Kearns, and P. R. Hanna, "The adaption of microwave heating to the rotational moulding process," in *SPE-ANTEC Annual Technical Conference: Proc. of the 68th Annual Technical Conference of the Society of Plastic Engineers 2010, ANTEC 2010*, Orlando, USA, 2010. pp. 1274-1278

[5] K. Von Kries, "System, method and apparatus for solar heated manufacturing," U.S. Patent 9 034 238, May 19, 2015.

[6] J. Olinek, C. Anand and C. Bellehumeur, "Experimental study on the flow and deposition of powder particles in rotational molding," *Polymer Engineering & Science*, vol. 45, no. 1, pp. 62-73, 2004. Available: 10.1002/pen.20230.

[7] S. Habib, "What is Rotational Molding | Rotational Molding Process | Advantages & Disadvantages | Best Material for Rotational Molding," PlasticRanger, 2021. [Online]. Available: https://plasticranger.com/what-is-rotational-molding/.

[8] M. P. McCourt and M. P. Kearns, "The development of internal water cooling techniques for the rotational moulding process," in *SPE-ANTEC Annual Technical Conference: Proc. of the 67th Annual Technical Conference of the Society of Plastic Engineers 2009, ANTEC 2009,* Chicago, USA, 2009. pp. 1961-1965.

[9] M. D. Marrero, P. Hernández, L. Suárez, D. Pestana, A. Benítez, J. Martín, S. Rivero, and E. Calero, "Rotational molding applied to the manufacturing of blades of small wind turbine," in *Proc. of the ASME 2014 12th Biennial Conference on Engineering Systems Design and Analysis*, Copenhagen, Denmark, 2014. pp. 1-5.

[10] M. Cramez, M. Oliveira and R. Crawford, "Optimisation of rotational moulding of polyethylene by predicting antioxidant consumption," *Polymer Degradation and Stability*, vol. 75, no. 2, pp. 321-327, 2002. Available: 10.1016/s0141-3910(01)00234-8.

[11] S. Liu and C. Ho, "Factors affecting the warpage of rotationally molded parts," *Advances in Polymer Technology*, vol. 18, no. 3, pp. 201-207, 1999. Available: 10.1002/(sici)1098-2329(199923)18:3<201::aid-adv1>3.0.co;2-n.

[12] A. Spence and R. Crawford, "The effect of processing variables on the formation and removal of bubbles in rotationally molded products," *Polymer Engineering & Science*, vol. 36, no. 7, pp. 993-1009, 1996. Available: 10.1002/pen.10487.

[13] W. Kingery and M. Berg, "Study of the Initial Stages of Sintering Solids by Viscous Flow, Evaporation-Condensation, and Self-Diffusion," Journal of Applied Physics, vol. 26, no. 10, pp. 1205-1212, 1955. Available: 10.1063/1.1721874.

[14] G. Kuczynski, "Study of the Sintering of Glass," Journal of Applied Physics, vol. 20, no. 12, pp. 1160-1163, 1949. Available: 10.1063/1.1698291.

[15] G. Kuczynski and I. Zaplatynskyj, "Sintering of Glass," Journal of the American Ceramic Society, vol. 39, no. 10, pp. 349-350, 1956. Available: 10.1111/j.1151-2916.1956.tb15601.x.

[16] C. T. Bellehumeur, "Polymer Sintering and its Role in Rotational Molding," Ph.D. dissertation, Dept. Chem. Eng., McMaster University, Hamilton, ON, Canada, 1997.

[17] O. Pokluda, C. Bellehumeur and J. Vlachopoulos, "Modification of Frenkel's model for sintering," *AIChE Journal*, vol. 43, no. 12, pp. 3253-3256, 1997. Available: 10.1002/aic.690431213.

[18] M. Narkis, "Sintering behavior of poly(methyl methacrylate) particles," *Polymer Engineering and Science*, vol. 19, no. 13, pp. 889-892, 1979. Available: 10.1002/pen.760191302.

[19] M. Rao and J. Throne, "Principles of rotational molding," *Polymer Engineering and Science*, vol. 12, no. 4, pp. 237-264, 1972. Available: 10.1002/pen.760120402.

[20] C. Bellehumeur, M. Kontopoulou and J. Vlachopoulos, "The role of viscoelasticity in polymer sintering," *Rheologica Acta*, vol. 37, no. 3, pp. 270-278, 1998. Available: 10.1007/s003970050114.

[21] J. Olinek, C. Anand and C. Bellehumeur, "Experimental study on the flow and deposition of powder particles in rotational molding," *Polymer Engineering & Science*, vol. 45, no. 1, pp. 62-73, 2004. Available: 10.1002/pen.20230.

[22] A. Greco and A. Maffezzoli, "Powder-shape analysis and sintering behavior of high-density polyethylene powders for rotational molding," *Journal of Applied Polymer Science*, vol. 92, no. 1, pp. 449-460, 2004. Available: 10.1002/app.20012.

[23] M. Kontopoulou and J. Vlachopoulos, "Bubble dissolution in molten polymers and its role in rotational molding," *Polymer Engineering & Science*, vol. 39, no. 7, pp. 1189-1198, 1999. Available: 10.1002/pen.11505.

[24] P. Y. Kelly, "A microscopic examination of rotomoulded polyethylene," *DuPont*, Toronto, Canada, 1981.

[25] S. Sarrabi, X. Colin and A. Tcharkhtchi, "Kinetic modeling of polypropylene thermal oxidation during its processing by rotational molding," *Journal of Applied Polymer Science*, p. n/a-n/a, 2010. Available: 10.1002/app.32459.

[26] P. Gijsman, "Review on the thermo-oxidative degradation of polymers during processing and in service," *e-Polymers*, vol. 8, no. 1, 2008. Available: 10.1515/epoly.2008.8.1.727.

[27] M. Oliveira, M. Cramez and R. Crawford, "Structure-properties relationships in rotationally moulded polyethylene," *Journal of Materials Science*, vol. 31, no. 9, pp. 2227-2240, 1996. Available: 10.1007/bf01152932.

[28] X. Colin and J. Verdu, "Polymer degradation during processing," *Comptes Rendus Chimie*, vol. 9, no. 11-12, pp. 1380-1395, 2006. Available: 10.1016/j.crci.2006.06.004.

[29] S. Liu and C. Ho, "Factors affecting the warpage of rotationally molded parts," *Advances in Polymer Technology*, vol. 18, no. 3, pp. 201-207, 1999. Available: 10.1002/(sici)1098-2329(199923)18:3<201::aid-adv1>3.0.co;2-n.

[30] S. Bawiskar and J. White, "Comparative study of warpage, global shrinkage, residual stresses, and mechanical behavior of rotationally molded parts produced from different polymers," *Polymer Engineering and Science*, vol. 34, no. 10, pp. 815-820, 1994. Available: 10.1002/pen.760341006.

[31] R. Pop-Iliev, C. B. Park, and K. H. Lee, "The Potentials for Processing Metallocene Polyethylene Grades in Rotational Molding," in *Proc. of the 18th Polymer Processing Society Conference*, Guimaraes, Portugal, 2002. p. 6.

[32] M. Oliveira and M. Cramez, "Rotational molding of polyolefins: Processing, morphology, and properties," *Journal of Macromolecular Science, Part B*, vol. 40, no. 3-4, pp. 457-471, 2001. Available: 10.1081/mb-100106170.

[33] H. Xu and C. Bellehumeur, "Thermal residual stress development for semi-crystalline polymers in rotational molding," *Polymer Engineering & Science*, vol. 48, no. 2, pp. 283-291, 2008. Available: 10.1002/pen.20887.

[34] G. Groeninckx, C. Harrats, M. Vanneste, and V. Everaert, "Crystallization, Micro- and Nano-structure, and Melting Behavior of Polymer Blends," in *Polymer Blends Handbook*, L. A. Utracki and C. A. Wilke, Eds. 2nd ed., Dordrecht: Springer Netherlands, 2014, ch. 3, pp. 291-446.

[35] R. Greco, C. Mancarella, E. Martuscelli, G. Ragosta and J. Yin, "Polyolefin blends: 2. Effect of EPR composition on structure, morphology and mechanical properties of iPP/EPR alloys", Polymer, vol. 28, no. 11, pp. 1929-1936, 1987. Available: 10.1016/0032-3861(87)90302-8.

[36] C. Chen, E. Fontan, K. Min and J. White, "An investigation of instability of phase morphology of blends of nylons with polyethylenes and polystyrenes and effects of compatibilizing agents," *Polymer Engineering and Science*, vol. 28, no. 2, pp. 69-80, 1988. Available: 10.1002/pen.760280203.

[37] S. F. Xavier, "Properties and Performance of Polymer Blends," in *Polymer Blends Handbook*, L. A. Utracki and C. A. Wilke, Eds. 2nd ed., Dordrecht: Springer Netherlands, 2014, ch. 10, pp. 1032-1201.

[38] L. Utracki, P. Mukhopadhyay and R. Gupta, "Polymer Blends: Introduction," *Polymer Blends Handbook*, pp. 3-170, 2014. Available: 10.1007/978-94-007-6064-6_3.

[39] L. M. Robeson, *Polymer Blends: A Comprehensive Review*. Munich, Germany: Hanser, 2007.

[40] A. J. Peacock, *Handbook of Polyethylene: Structures, Properties, and Applications*. New York, NY: Marcel Dekker, 2000.

[41] L. A. Utracki, G. Z.-H. Shi, D. Rodrigue, and R. Gonzalez-Núñez, "Compounding Polymer Blends," in *Polymer Blends Handbook*, L. A. Utracki and C. A. Wilke, Eds. 2nd ed., Dordrecht: Springer Netherlands, 2014, ch. 9, pp. 919-1028.

[42] L. A. Utracki, "The Rheology of Multiphase Systems," in *Rheological Fundamentals of Polymer Processing*, J. Covas, J. Agassant, A. Diogo and J. Vlachopoulos, Eds. Dordrecht: Springer Netherlands, 2010, pp.113-137.

[43] P. Walia, R. Gupta and C. Kiang, "Influence of interchange reactions on the crystallization and melting behavior of nylon 6,6 blended with other nylons," *Polymer Engineering & Science*, vol. 39, no. 12, pp. 2431-2444, 1999. Available: 10.1002/pen.11631.

[44] M. Doi and A. Onuki, "Dynamic coupling between stress and composition in polymer solutions and blends", *Journal de Physique II*, vol. 2, no. 8, pp. 1631-1656, 1992. Available: 10.1051/jp2:1992225.

[45] F.N. Cogswell, B.P. Griffin, and J.B. Rose, "Compositions of melt-processable polymers having improved processability," U.S. Patent 4 386 174, May 31, 1983.

[46] R. Steller and D. Żuchowska, "Free volume theory for rheological properties of polymer blends," *Journal of Applied Polymer Science*, vol. 41, no. 78, pp. 1595-1607, 1990. Available: 10.1002/app.1990.070410719.

[47] P. Couchman, "The viscosity of miscible blends," *Journal of Applied Polymer Science*, vol. 60, no. 7, pp. 1057-1060, 1996. Available: 10.1002/(sici)1097-4628(19960516)60:7<1057::aid-app17>3.0.co;2-y.

[48] A. Ajji, "Interphase and Compatibilization by Addition of a Compatibilizer," in *Polymer Blends Handbook*, L. A. Utracki and C. A. Wilke, Eds. 2nd ed., Dordrecht: Springer Netherlands, 2014, ch. 4, pp. 447-516.

[49] L. Utracki, *Polymer alloys and blends*. Munich: Hanser, 1990.

[50] R. Pasquali, M. Taurozzi and C. Bregni, "Some considerations about the hydrophilic–lipophilic balance system", *International Journal of Pharmaceutics*, vol. 356, no. 1-2, pp. 44-51, 2008. Available: 10.1016/j.ijpharm.2007.12.034.

[51] W. C. Griffin, "Classification of Surface-Active Agents by "HLB"," *Journal of Cosmetic Science*, vol. 1, pp. 311-326, 1949.

[52] A. Gadhave, "Determination of Hydrophilic-Lipophilic Balance Value," *International Journal of Science and Research (ISJR)*, vol. 3, no. 11, pp. 573-575, 2014. Available: https://www.ijsr.net/archive/v3i4/MDIwMTMxNTMw.pdf.

Chapter 3. Experimental

3.1 Materials

High-density polyethylene ($HDPE\ HD\ 8660.29$) and polyamide 11 ($Rilsan®\ PA11$) were supplied by Imperial Oil Ltd. (Sarnia, ON). Melting point temperature T_m, crystallisation point temperature T_c, heat of fusion ΔH_m, and enthalpy at crystallisation, ΔH_c for $HDPE$ and $PA11$ are given in Table 3.1. The particle size distribution is given in Figure 3.1.

Table 3.1. Thermal behaviour of neat $HDPE$ and $PA11$.

	T_m (℃)	$\Delta H_m \left(\frac{J}{g}\right)$	T_c (℃)	$\Delta H_c \left(\frac{J}{g}\right)$
HDPE	121.90 ± 0.16	162.43 ± 2.45	116.06 ± 0.08	159.11 ± 3.07
PA11	177.23 ± 0.29	47.83 ± 0.82	161.79 ± 0.18	45.68 ± 0.41

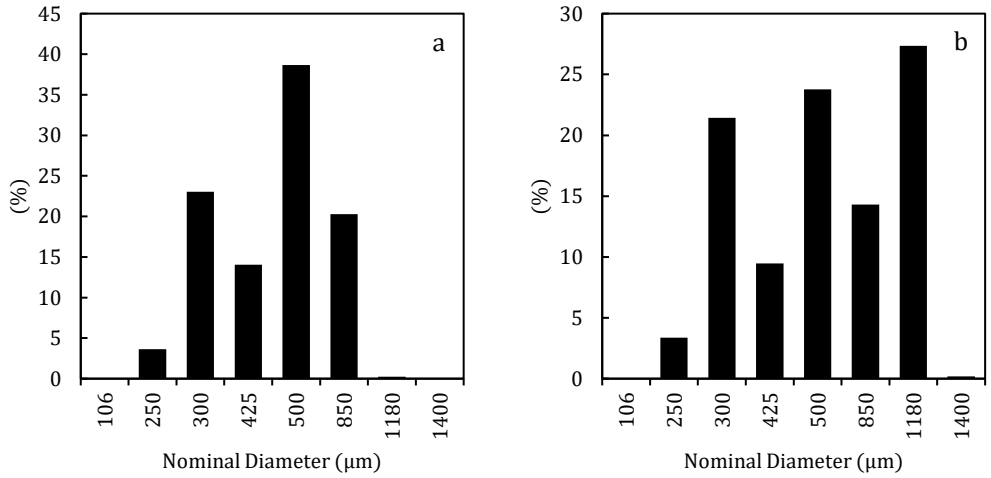

Figure 3.1. Particle size distribution of $HDPE$ [a] and $PA11$ [b] determined as percentage of total mass passing through each sieve via sieve analysis.

Surface-active non-ionic surfactants, sorbitan trioleate (Span® 85, HLB = 1.8 ± 1.1), sorbitan monostearate (Span® 60, HLB = 4.7), polyoxyethylene sorbitan monostearate (Tween® 60, HLB = 14.9), and poly(ethylene glycol)-*block*-

poly(propylene glycol)-*block*-poly(ethylene glycol) (Pluronic® F-108, HLB = 27) were supplied by Sigma-Aldrich (Mississauga, ON). Polyoxyethylene sorbitan monolaurate (Tween® 20, HLB = 16.7) was supplied by VWR International (Mississauga, ON). Flocculating agent, deacetylated chitin (Chitosan, HLB = 36.7 [1]) was supplied by Sigma-Aldrich (Mississauga, ON). Compatibilizer, pelletized acrylic acid-functionalised high-density polyethylene (Polybond 1009, supplied by Chemtura) was cryogenically ground to ≤ 500 μm by Ingenia Polymers Corp. (Brantford, ON). Etching agents, formic acid and xylene were supplied by Sigma-Aldrich (Mississauga, ON). Isopropanol was supplied by Fisher Scientific (Mississauga, ON).

3.2 Methods

3.2.1 Particle Coalescence

Sintering behaviour and particle coalescence were observed via hot-stage microscopy. The apparatus was comprised of an aluminum microslide stage, primarily heated via conduction using an aluminum heating block enwrapped within a heating element, as shown in Figure 3.2. Particles ≤ 500 μm were placed on the microslide and heated at a rate of 2.8 ˚C/min. Images were captured via optical microscopy using a stereo microscope (Olympus Corporation; Richmond Hill, ON), every 30 seconds from 75 °C to 250 °C. The temperature was recorded at the surface of the aluminum microslide .

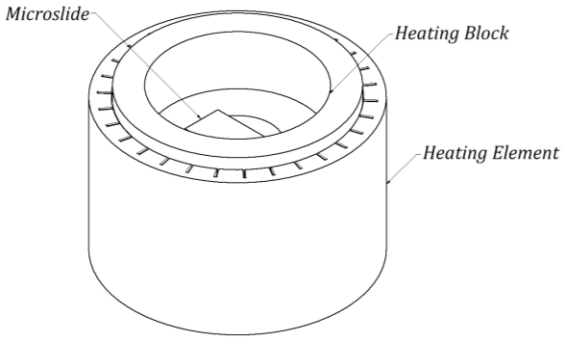

Figure 3.2. Hot-stage microscopy apparatus for qualitative observation of sintering behaviour and predictive coalescence.

3.2.2 Blend Preparation

3.2.2.1 Dry-Blended

Tween 20 and Span 85 compatibilizing surfactants prepared for direct-mixing were diluted with 10 mL of isopropanol inside 50 mL Falcon Conical Centrifuge Tubes and vortex mixed for 2 minutes. $HDPE$, $PA11$, and the diluted surfactant were then manually mixed using a PRODUKT milk-frother (IKEA; Etobicoke, ON) for 5 minutes directly within the rotomolding mold cavity, and dried uncovered in a VWR® Vacuum Oven at a temperature of T_{VAC} = 35 °C for 6 hours as shown in Figure 3.4a. The mold was thereafter retrieved from the oven, sealed on both ends, and affixed to the rotomolding axle as shown in Figure 3.4b.

3.2.2.2 Extrusion-Blended

Surfactant-coated $HDPE$ particles were prepared using a G.U.N.T. Hamburg WL 255 fluidised bed reactor retrofitted with a McMaster-Carr 32215K11 full-cone no-drip misting nozzle as shown in Figure 3.2. Dilute Tween 20 solution was top-sprayed on 90 g of fluidised $HDPE$ particles at a spray angle, ϑ = 70° and mass

flow-rate, $\dot{m}_{FBR}$ = 0.339 $\frac{g}{s}$ for t_{FBR} = 10 seconds, with theoretical droplet particles ranging from 31 to 41 μm in diameter. Surfactant solution was fed to the spray nozzle using a LMI Milton Roy microprocessor dosing pump.

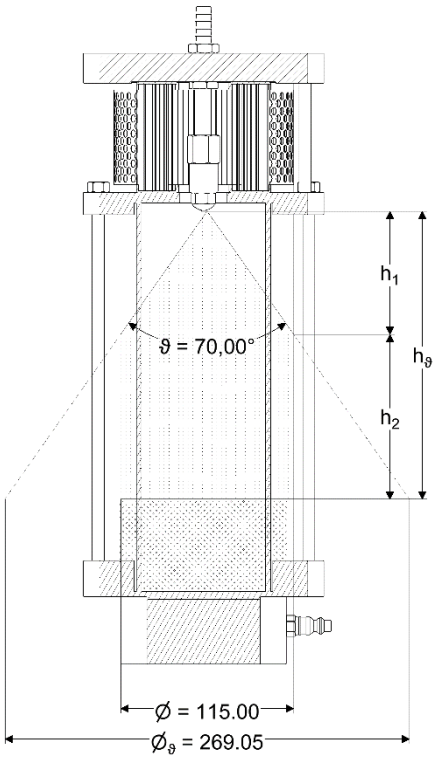

Figure 3.3. Top-spray retrofitted fluidised bed reactor for spray coating $HDPE$ particles with dilute Tween 20 surfactant.

To calibrate the process, a Beckman Coulter DU 800 Spectrophotometer was used for ultraviolet-visible (UV-VIS) spectroscopy to accurately determine the concentration of Tween 20 in the fluidised bed reactor feed solution. Samples of 0.5 wt%, 1.0 wt%, 2.0 wt%, 5.0 wt%, and 10.0 wt% Tween 20 diluted with distilled water were prepared using a Mettler Toledo AE200 Analytical Balance and mixed using a VWR® Mini Vortex Mixer for 120 seconds. These samples were

transferred into StonyLab Scientific (Nesconset, NY) quartz cuvettes and scanned at a wavelength interval of 0.1 nm and scan speed of 120 nm/min, over a range of 200.0 to 300.0 nm as shown in Figure 3.3a. A concentration of Tween 20, $m_{T_{20}|FBR}$ = 10.98 wt% in the feed solution was determined using the calibration curve shown in Figure 3.3b, at an absorbance wavelength of 280 nm.

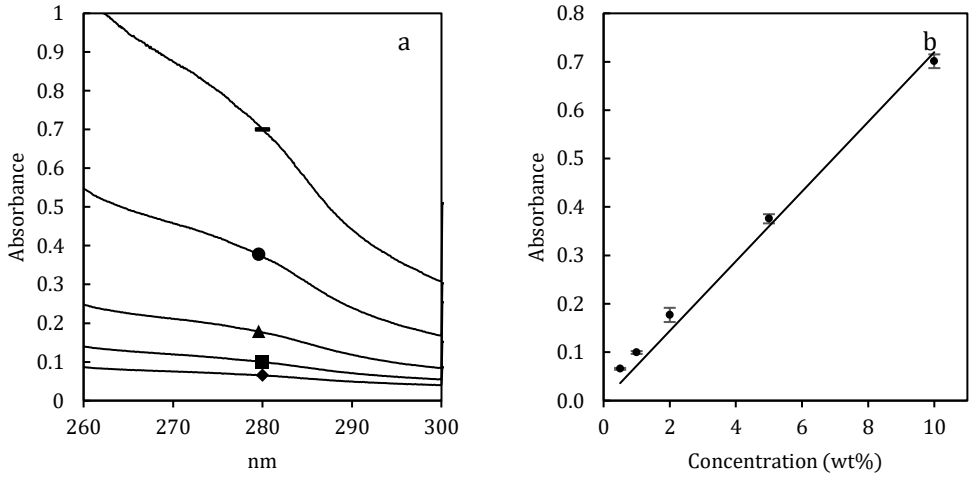

Figure 3.4. UV-VIS absorbance curves for 0.5% (◆), 1.0% (■), 2.0% (▲), 5.0% (●), and 10.0% (▬) polyoxyethylene (20) sorbitan monolaurate [a] and absorbance calibration curve at 280 nm, where absorbance, $A = 0.072 \times C_{T_{20}}$ [b].

A correction factor, c was used to accurately predict the amount of surfactant deposited onto fluidised $HDPE$ particles given by,

$$c = \frac{v}{v_\vartheta} \tag{3.1}$$

where,

$$v = \frac{1}{3}\frac{\pi\left(\frac{\phi}{2}\right)^3}{\tan\left(\frac{\vartheta}{2}\right)} + \pi\left(\frac{\phi}{2}\right)^2 h_\vartheta - \frac{\pi\left(\frac{\phi}{2}\right)^3}{\tan\left(\frac{\vartheta}{2}\right)} \ (mm^3) \tag{3.2}$$

and,

$$v_{\vartheta} = \frac{1}{3}\pi h_{\vartheta}^{3} \tan^{2}\left(\frac{\vartheta}{2}\right) \ (mm^{3}) \tag{3.3}$$

This resulted in a surfactant coating of, $w_{T_{20}|TSE}$ = 0.122% in both the 50/50 and 75/25 Tween 20 coated $HDPE\text{-}PA11$ extruded blends, where,

$$w_{T_{20}|TSE} = t_{FBR} c\dot{m}_{FBR} \frac{m_{T_{20}{}_{FBR}}}{m_{HDPE_{FBR}} + m_{T_{20}{}_{FBR}}} \ (\%) \tag{3.4}$$

Coated and uncoated $HDPE\text{-}PA11$ extruded blends were prepared using a 27 mm 40 L/D Leistritz ZSE-27HP co-rotating twin-screw extruder (Leistritz Advanced Technologies Corp.; Somerville, NJ) at a uniform barrel temperature of 215 °C, screw speed of 200 RPM, and a feed-rate of 5 $\frac{kg}{hr}$. A PX-MFC 90 D laboratory mill by Kinematica, Inc. (Bohemia, NY) with a 500 μm sieve was used to grind extruded material at 3000 ± 100 RPM for rotomolding.

3.2.3 Rotomolded Physical Blends

Characterisations and comparative analyses were completed on rotomolded physical blends prepared via the two types of aforementioned compounding and mixing techniques:

1. *Dry-blending*, where $HDPE$, $PA11$, and compatibilizers Tween 20 or Span 85 are dry-mixed manually inside the mold cavity and melt phase mixing takes place exclusively within a single rotomolding cycle (*see § 3.2.2.1*).
2. *Melt-blending*, where $HDPE$, $PA11$, and Tween 20 are melt-mixed under high shear via twin-screw extrusion, then ground to a desired particle size (< 500

μm), and thereafter rotomolded under the same rotomolding conditions as the dry-mixed blends (*see § 3.2.2.2*).

Both dry- and melt-blended formulations were uniaxially rotomolded in a cuboid Teflon®-coated aluminum mold measuring 95 ± 5 mm length in every dimension. Enclosed within the oven, the mold was then rotated at a rate of 4 RPM with the platens set-point temperature, $T_{SP|URM}$ = 300 °C and peak internal air temperature, $PIAT$ = 235 °C, with an average heating rate of $\dot{\bar{r}}_{h|URM}$ = 0.185 ± 0.017 $\frac{^{\circ}C}{s}$ and an average cooling rate of $\dot{\bar{r}}_{c|URM}$ = 0.223 ± 0.011 $\frac{^{\circ}C}{s}$ as shown in Figure 3.4c. Complete variables of study are listed in Table 3.2.

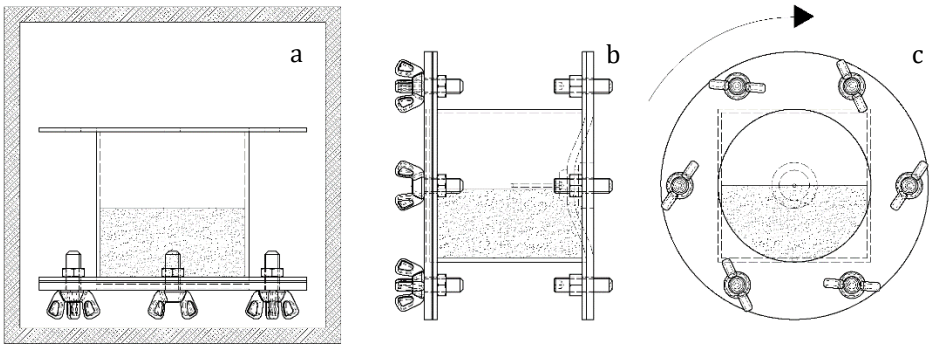

Figure 3.5. Rotomolded blends directly-mixed within the mold cavity and dried inside a vacuum oven [a]; sealed mold cavity affixed to the rotating axle [b]; mold enclosed inside the rotomolding oven rotating at 4 RPM until $PIAT$ = 235 °C [c].

Table 3.2. Complete list of rotomolded physical blend systems investigated.

SYSTEM	w_P (%)		w_s (%)		MIXING STRATEGY
	HDPE	PA11	Tween 20	Span 85	
HDPE	100	-	-	-	Dry
PA11	-	100	-	-	Dry
50/50	50	50	-	-	Dry
75/25	75	25	-	-	Dry
50/50/0.1-T20	50	50	0.1	-	Dry
50/50/0.5-T20	50	50	0.5	-	Dry
50/50/1-T20	50	50	1.0	-	Dry
50/50/1-S85	50	50	-	1.0	Dry
75/25/0.1-T20	75	25	0.1	-	Dry
75/25/0.5-T20	75	25	0.5	-	Dry
75/25/1-T20	75	25	1.0	-	Dry
75/25/1-S85	75	25	-	1.0	Dry
50/50-EXT	50	50	-	-	Extrusion
75/25-EXT	75	25	-	-	Extrusion
50/50/0.1-T20-EXT	50	50	0.1	-	Extrusion
75/25/0.1-T20-EXT	75	25	0.1	-	Extrusion

Specimens for Izod impact testing, flexural testing, density, and morphological characterisation were cut from four walls of the rotomolded cuboids, as shown in Figure 3.5a and according to ASTM standards where applicable. The pendulum for Izod impact testing struck the cross-sectional region designated by the hatch pattern in Figure 3.5b, where S_i and S_e denote the internal and external surfaces, respectively. While flexural testing, the internal surface, S_i rests on two supports and load is applied across the external surface, S_e. The depth of the cross-sectional (hatched) region shown in Figure 3.5b was measured by averaging the

widest points measured across half-widths of the rectangular specimens, designated d_1 and d_2 as shown in Figure 3.5c. Morphological characterisation via optical microscopy was done on etched regions of the (hatched) cross-section in Figure 3.5b.

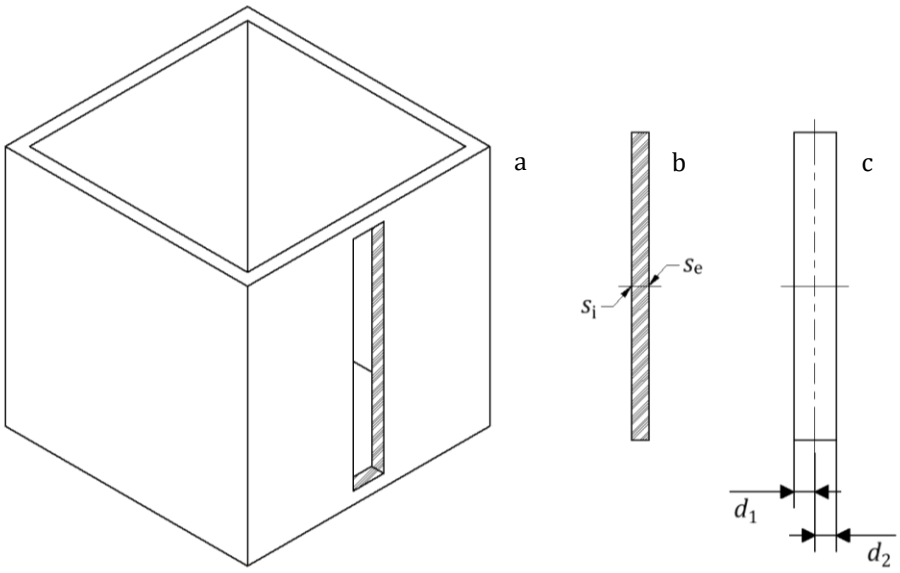

Figure 3.6. Rectangular specimens cut from 4-sided rotomolded cuboids [a], cross-sectional region of rectangular specimens [b], and surface view of rectangular specimens [c].

3.3 Characterizations

3.3.1 Density and Porosity

Porosity, f for rotomolded samples is given by,

$$f = 1 - \frac{\rho_{URM}}{\rho_{CM}} = 1 - \frac{\rho_{URM}\left(\frac{w_{HDPE}}{w_{PA11}}\right)}{\left[\frac{w_{HDPE}}{\rho_{CM(HDPE)}} + \frac{w_{PA11}}{\rho_{CM(PA11)}}\right]^{-1}} \ (\%) \qquad (3.5)$$

where, ρ_{URM} is the density of rotomolded samples and ρ_{CM} is the density of compression molded samples.

Compression molded samples for neat $HDPE$ and $PA11$ were prepared according to ASTM D4703 using a Carver 4389 benchtop manual press with electrically heated platens (Wabash, IN) at 135 °C and 215 °C, respectively. Densities of both, compression and rotomolded specimens were measured using a Mirage MD-200S electronic densimeter at 21 °C via Archimedes' principle. Densities of compression molded samples of $HDPE$ and $PA11$ were determined to be 0.941 ± 0.004 $\frac{g}{cm^3}$ and 1.053 ± 0.015 $\frac{g}{cm^3}$, respectively.

3.3.2 Thermal Properties

Thermal properties of $HDPE$, $PA11$, and blends thereof were determined using TA Instruments' Q200 differential scanning calorimeter (Grimsby, ON) with a sample size of 7.5 ± 1.0 mg sealed in Tzero aluminum hermetic pans at a heating and cooling ramp rate of, $\dot{r}_{DSC} = 5\ \frac{^{\circ}C}{min}$. $HDPE$ samples were heated from 25 °C to 175 °C, cooled to -80 °C, and then heated to 250 °C. All other samples were heated from 25 °C to 215 °C, cooled to -80 °C, and then heated to 250 °C.

3.3.3 Particle Size Analysis

Particle size distributions were determined using a RO-TAP® RX-29 test sieve shaker (W.S. Tyler; Mentor, OH). Samples were agitated via circular (horizontally) and tapping (vertically) motion for 30 minutes, across sieve sizes of 106, 250, 300, 425, 500, 850, 1180, and 1400 μm nominal openings. The weight difference of each sieve before and after the sieving cycle is represented as the particle size distribution.

3.3.4 Infrared Analysis

Thermo Scientific Nicolet 6700 Fourier-Transform Infrared Spectrometer (FT-IR) was used in attenuated total reflectance (ATR) mode on neat $HDPE$ and $PA11$ rotomolded specimens with $PIAT$ = 225 °C, 235 °C, and 240 °C to determine the onset of thermal degradation via the presence of non-characteristic peaks. An average of 64 scans at a resolution of 0.1 cm^{-1} were reported over a range of mid-infrared radiation wavenumbers (500 to 4000 cm^{-1}).

3.3.5 Impact Strength and Modified Izod Impact Test

Rectangular specimens were cut and tested according to Test Method A of ASTM D256 standard using a ZwickRoell HIT25P pendulum impact tester (Kennesaw, GA) with a maximum impact energy limit of 5.5 J and test specimen temperature, T_{I_s} = 21 °C. The impact test specimens deviated from the standard by neglecting the standardised notch dimensions. Samples were instead notched using Feather Microtome S35 Type blades at a notching depth of 2.54 ± 0.25 mm. The impact strength I_s is given by,

$$I_s = \frac{E_s - E_{TC}}{t} \left(\frac{J}{m}\right) \tag{3.6}$$

where E_s represents specimen breaking energy, E_{TC} represents total correction energy for the specimen breaking energy, and t represents the width of the specimen. Results are reported as the specific impact strength I_s^* where,

$$I_s^* = \frac{I_S}{\rho} \left(\frac{J \cdot m^2}{g}\right) \tag{3.7}$$

3.3.6 Three-Point Flexural Testing

Flexural strength/stress, σ_f of rectangular rotomolded specimens was determined via Procedure A of ASTM D790 standard using an Instron 3366 Universal Testing System (Norwood, MA). Flexural strength is determined by,

$$\sigma_f = \frac{3PL}{2bd^2}\ (MPa) \tag{3.8}$$

where, P represents the load at a given point on the load-deflection curve, b and d are the width and depth of the specimen, respectively, and length of the support span, L = 30 mm. . Results are reported as the specific impact strength I_s^* where,

$$\sigma_f^* = \frac{\sigma_f}{\rho}\left(\frac{MJ}{g}\right) \tag{3.9}$$

The rate of crosshead motion, R was determined by,

$$R = \frac{ZL^2}{6d}\left(\frac{mm}{min}\right) \tag{3.10}$$

where, the rate of straining of the outer fiber, Z = 0.01.

3.3.7 Morphological Analysis

50/50 and 75/25 $HDPE$-$PA11$ coated, uncoated, and pre-extruded rotomolded specimens were etched using xylene and formic acid, respectively. 50/50 specimens were immersed in xylene-filled glass tubes inside a continuously stirred silicone oil (Sigma-Aldrich) bath at 125 °C for 24 hours, to etch away the continuous $HDPE$ phase. Similarly, 75/25 specimens were immersed in formic acid-filled glass tubes inside a continuously stirred silicone oil bath at 95 °C for 24 hours, to etch away the dispersed $PA11$ phase. After removal from the etching

solutions, the samples were rinsed with isopropanol and distilled water to remove etchant residue. The morphology of the etched regions was observed via optical microscopy using a stereo microscope (Olympus Corporation; Richmond Hill, ON).

3.3.8 Zero-Shear Viscosity

Tween 20 coated $HDPE$ and $PA11$ samples were prepared by first depositing a uniform layer of polymer particles inside a petri-dish, and then immersing the layer of particles with a Tween 20 solution diluted using isopropanol at surfactant concentrations of 0.1 wt%, 0.5 wt%, or 1.0 wt%. The petri dishes were then placed on an oscillating shaker for 48 hours at ambient room temperature, allowing for the isopropanol to evaporate and for the polymer particles to be uniformly coated. A Discovery Hybrid Rheometer HR-2 (TA Instruments; Grimsby ON) was used for all rheological characterisations using steel electrically heated plates in a 25 mm parallel plate configuration.

A logarithmic flow-ramp (30 points per decade) was used for coated and uncoated $HDPE$ particles with a geometry gap of 1000 μm at 235 °C for 180 seconds over a shear rate range of 0.01 to 100 $\frac{1}{s}$. A continuous oscillation logarithmic frequency sweep (35 points per decade) was used for coated and uncoated $PA11$ particles with a geometry gap of 500 μm at 235 °C and 5% strain, over a frequency range of 1 to 100 $\frac{1}{s}$. A Cox Merz transformation was applied to the frequency sweep output to generate a shear rate – viscosity curve. Zero-shear

viscosity for all rheology specimens was predicted using the Carreau-Yasuda model where,

$$\eta_{CY} = \frac{\eta_0}{[1 + (\lambda\dot{\gamma})^a]^{\frac{1-n}{a}}} \tag{3.11}$$

and validated using the Cross model where,

$$\eta_C = \frac{\eta_0}{1 + \left(\frac{\eta_0\dot{\gamma}}{\tau^*}\right)^{[1-n]}} \tag{3.12}$$

3.4 References

[1] P. Schulz, M. Rodríguez, L. Del Blanco, M. Pistonesi and E. Agulló, "Emulsification properties of chitosan," *Colloid & Polymer Science*, vol. 276, no. 12, pp. 1159-1165, 1998. Available: 10.1007/s003960050359.

Chapter 4. Results and Discussion

4.1 Crystallisation Kinetics and Immiscibility

Crystallisation kinetics and melting properties of polymer blends are dependent on intermolecular interactions in the interphase and the miscibility of the constituent polymer components [1], [2]. The glass transition temperature, T_g has been shown to be insensitive to the thermodynamic immiscibility of a multiphasic polymer blend [3]. Therefore, the analysis of the thermal behaviours herein of $HDPE$ and $PA11$, and blends thereof is limited to the melting and crystallisation peaks.

As shown in Figure 4.1a and b, the straight and narrow melting and crystallisation peaks for homopolymers $HDPE$ and $PA11$, respectively, are representative of semi-crystalline polymers with no eutectic impurities present. The melting temperatures of pure $HDPE$ and $PA11$ are 121.90 °C and 177.23 °C, respectively. The melting process (*red*) for $HDPE$ shows an exothermic peak at approximately 240 °C, with the onset at around 235 °C suggesting mild, albeit negligible degradation. Whereas $PA11$ is shown to remain thermally stable at temperatures up to 245 °C, with only an endothermic peak is observed around the melting point. The enthalpies of melting, ΔH_f of $HDPE$ and $PA11$ were 164.48 $\frac{J}{g}$ and 47.62 $\frac{J}{g}$, respectively. The melting enthalpy for pure 100% crystalline samples, $\Delta H_{f_{100\%}}$ of $HDPE$ is 293 $\frac{J}{g}$ whereas it is 244 $\frac{J}{g}$ for $PA11$ [4]. Homopolymers, $HDPE$ and $PA11$ were determined to have a crystallinity of 56% and 19.5%, with a weight fraction, $w = 1$, where percent crystallinity is given by:

$$(1-\lambda)\% = \frac{\Delta H_f}{\Delta H_{f_{100\%}} \cdot w} \times 100 \tag{4.1}$$

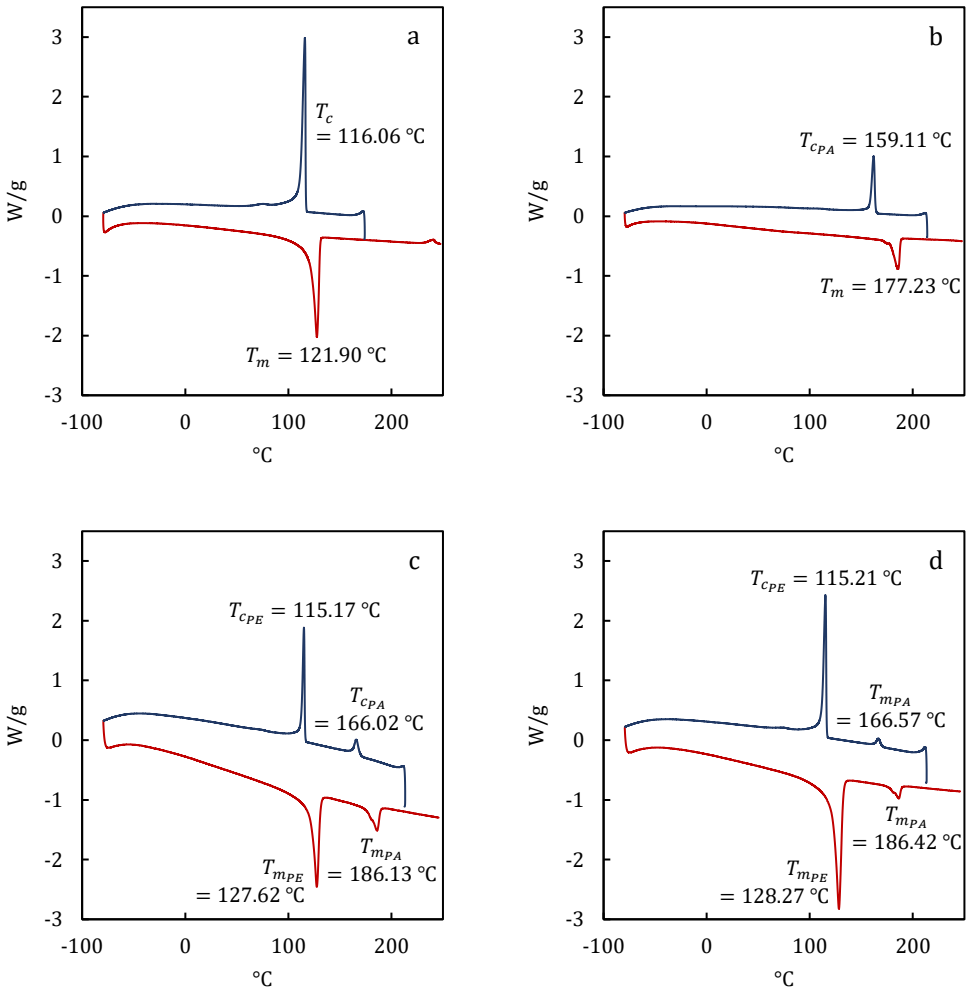

Figure 4.1. Characterisation of thermal behaviour via differential scanning calorimetry (exotherm up) of $HDPE$ [a], $PA11$ [b], 50/50 $HDPE$-$PA11$ [c], and 75/25 $HDPE$-$PA11$ [d].

Inter-polymer chain entanglements in polymer blends are limited by the thickness of the interface between the continuous matrix and the dispersed phase in biphasic polymer blends. This interfacial region, referred to as the interphase, is particularly narrow for multiphase, thermodynamically immiscible blends [5].

Consequently, the lack of entanglement between the non-polar $HDPE$ and polar $PA11$ phases results in poor interfacial adhesion. Therefore, immiscibility in polymer blends is inextricably linked to poor mechanical properties [1]. The interfacial phenomenology of the interphase in immiscible polymer blends is understood to be codependently correlated to the crystallisation behaviour of the constituent components or more specifically to their crystallisation temperatures [1]. The blend composition/ratio has been shown to influence the crystallisation rate of the constituent polymers, which is characteristically defined by the number of active nuclei or primary nucleation at the interphase and the crystal growth rate [6]. Changes in the crystallisation temperature elicited by varying blends ratios of the constituent polymers can explain the increase or decrease in the number of active nuclei and the onset of smaller, finer dispersions of one component within the continuous matrix of the other [1].

Figures 4.1c and d show the effect of simultaneous melting and crystallisation on the thermal behaviours of $HDPE$ and $PA11$ in 50/50 and 75/25 $HDPE$-$PA11$ blends, respectively. In the 50/50 blend, the melting points for $HDPE$ and $PA11$ increased by 6 °C and 9 °C, respectively compared to the homopolymers, whereas a negligible increase of 1 °C and a relatively significant increase of 7 °C was observed for the crystallisation temperatures of $HDPE$ and $PA11$, respectively. The 75/25 blend showed a similar trend, except that the melting point temperature for $HDPE$ increased by an equally negligible 2 °C. The presence of separated crystallisation peaks is not uncommon for thermodynamically immiscible polymer

blends, as has been shown for polyamide 6 – polypropylene and polyamide – low-density polyethylene blends. Moreover, Chen et al [7] reported that there was no discernable difference in the melting point of the dispersed $PA11$ phase in their 75/25 $HDPE$-$PA11$ blends. The increase in the melting point temperature of $HDPE$ can be attributed to the high heat absorptivity of $PA11$. The presence of $PA11$ therefore, results in the delayed onset of melting of the $HDPE$ crystals. As the temperature increased, most of the solid $PA11$ particles were assumed to be dispersed within the $HDPE$ melt.

The deviation in the cooling or crystallisation behaviour of $PA11$ is not uncommon and the crystallisation temperature, T_c has been shown to shift due to the migration of heterogeneities between the dispersed and continuous phases in semicrystalline polyblends [8]. The other factor commonly associated with a change in T_c is the nucleation of crystals at the interphase. This however is not likely for $PA11$, because $HDPE$ should not exhibit any nucleating activity on the polyamide at 186 °C.

The change in the thermal behaviour however does have an effect on the resultant phase dispersion morphology and consequently, the blend's mechanical properties [9]. Recall that during mixing, the blend phase equilibrium is driven by concurrent coalescence and dispersion mechanisms [10]. For the purposes of this discussion, *coalescence* describes the tendency of like particles to aggregate or flocculate during mixing. Whereas *dispersion* describes the spreading of the dispersed phase (i.e. $PA11$) within the continuous matrix (i.e. $HDPE$) in a zero-

shear environment. Furthermore, recall from *§ 2.2.2* that the dispersion and coalescence models given by equations (2.2) and (2.3), respectively, model the change in spherical droplet diameter as a function of time. An increase in T_m and T_c of 9 C° and 7 °C, respectively means that the mixing window for $PA11$ decreases by 16 °C. Using the experimental rotomolding heating and cooling rates (*§ 3.2.3*), the presence of $HDPE$ is determined to result in a 16% and 10% decrease in the melting and densification times for $PA11$, respectively. Therefore, it is likely that $PA11$ will not reach a minimum drop diameter as the dispersed phase since there is a limited window for droplet breakup. Instead, the relatively larger droplets (compared to the thermal cycle for a $PA11$ homopolymer) will coalesce, forming larger continuous regions and eliciting phase separation as result. This phenomenon as shown in *§ 4.5.1*, is more prominent in the 50/50 dry-mixed blend compared to the 75/25 dry-mixed blend due to the increased weight percentage of $PA11$, although mechanical compatibilization via twin-screw extrusion yielded different results.

The melting peaks for both 50/50 and 75/25 blends were broader relative to those of the homopolymers. This is due the reduction of crystallinity and an increase in the amorphous region in both $HDPE$ and $PA11$. This observation is corroborated by a decrease in percent crystallinity for the constituent components of the polyblends. For the 50/50 blend, the melting enthalpies of $HDPE$ and $PA11$ were 64.94 $\frac{J}{g}$ and 16.99 $\frac{J}{g}$, respectively, and 114.00 $\frac{J}{g}$ and 8.1928 $\frac{J}{g}$ for $HDPE$ and $PA11$, respectively, in the 75/25 blend. Compared to the homopolymer at 56%, the percent

crystallinity of $HDPE$ decreased and was determined to be 44.3% and 51.9% for the 50/50 and 75/25 blends, respectively. Whereas for $PA11$, percent crystallinity decreased from 19.5% for the homopolymer to 13.9% and 13.4% for the 50/50 and 75/25 blends, respectively. In both scenarios, the percent crystallinity decreases due to a decrease in the alignment of like stereoregular regions of $HDPE$ and $PA11$ chains. The intermolecular interactions via entanglement of the immiscible non-polar $HDPE$ and polar $PA11$ chains in the melt phase, inhibit the rearrangement of these chains into ordered crystalline regions upon densification/solidification.

4.2 Thermal Degradation of High-Density Polyethylene

Rotomolded samples of pure $HDPE$ and $PA11$ were tested for thermal oxidative degradation. Figure 4.2 shows both the reference and the degradation bands for $HDPE$. The reference bands are coloured black and the degradation bands are coloured red. The onset of thermo-oxidative degradation of $HDPE$ is demonstrated by the presence of degradation bands at 1,716 cm^{-1}, 1,227 cm^{-1}, and 1,156 cm^{-1}. These results validated the apparent yellowish discolouration of rotomolded $HDPE$ consistently seen at temperatures greater than 235 °C. Furthermore, an exothermic peak at approximately 240 °C was also observed in the melting stage of the DSC curve for $HDPE$ (*see § 4.1*). Comparatively, as shown in Figure 4.3, $PA11$ showed no distinct degradation peaks compared to the reference ATR-FTIR spectra. This is consistent with the DSC curve for the thermal behaviour of $PA11$, where no exothermic peaks were observed and the molten resin was stable even at a temperature of 245 °C.

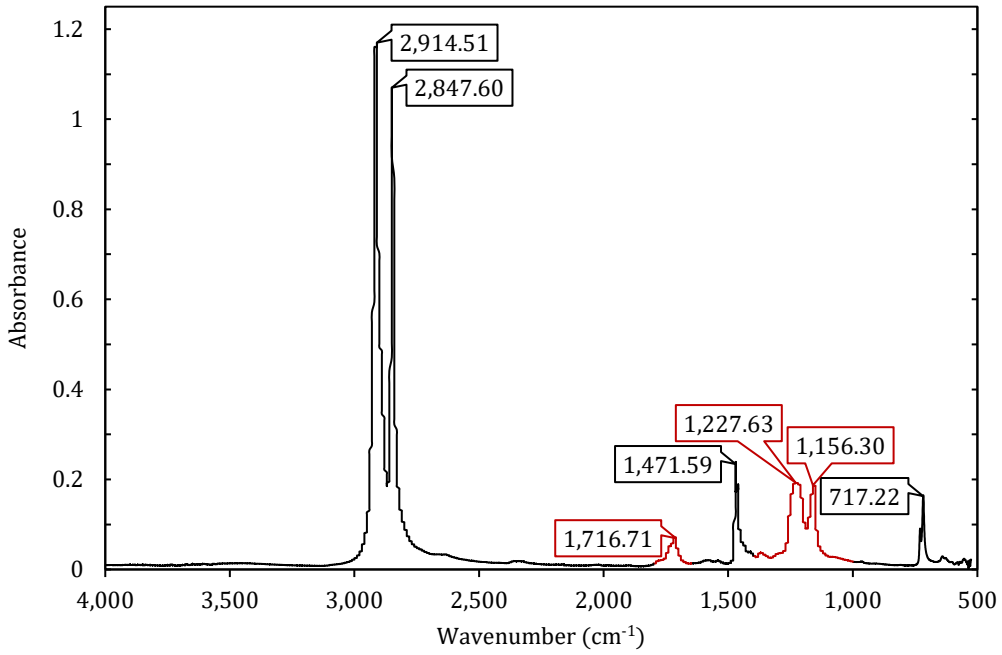

Figure 4.2. ATR-FTIR spectra for $HDPE$ rotomolded to $PIAT$ = 240 °C; baseline characteristic peaks are shown in *black* and peaks representative of thermal degradation are shown in *red*.

The balance between operating rotational molding processes at low and high values of $PIAT$ is of paramount importance. Low values of $PIAT$ can result in improper or incomplete diffusion of gasses following the densification step of the rotomolding cycle [11]. This translates into the entrapment of air (bubble formation) resulting in poor mechanical properties, such as low impact strength and the apparent brittle failure of rotomolded articles [12], [13]. Furthermore, rotomolded $HDPE$ has been shown to exhibit a favourable and proportional improvement in mechanical properties and more specifically, impact strength as a function of increasing $PIAT$ [14]. However, very high values of $PIAT$ can elicit thermo-oxidative degradation, which change the surface morphology and cause a

deterioration of mechanical properties. Therefore, in both $HDPE$-based blends covered by the study, the ideal $PIAT$ value was consistently determined to be just prior to the onset of degradation [11], which was 235 °C.

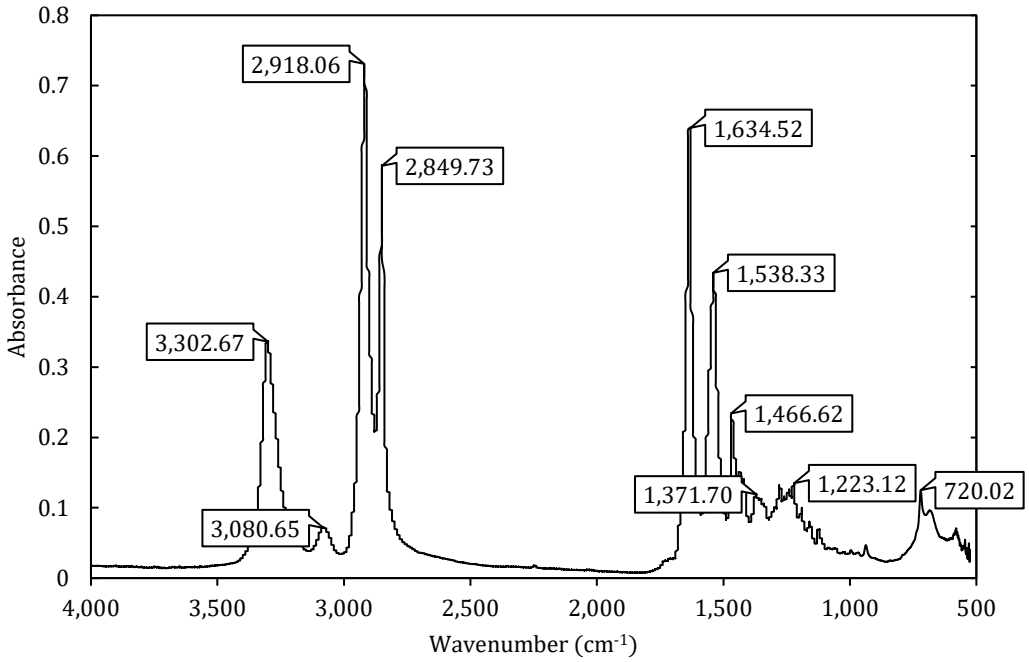

Figure 4.3. ATR-FTIR spectra for $PA11$ rotomolded to $PIAT$ = 240 °C.

4.3 Sintering and Interparticle Cohesion

Inherent weakness in rotomolded parts of physical immiscible blends are attributed to bubble formation and weak domain adhesion [15]; due to low diffusive motion and no convective motion in the process, a domain (or droplet) in this case corresponds to dimensions similar to the original powder. For the purposes of this discussion, *coalescence* is used to describe the unification of spherical droplets of the same polymer during heating, whereas *cohesion* is used to describe interfacial adhesion between $HDPE$ and $PA11$ particles. In the case of a physical blend, two

adjacent particles in a bed may be of different composition and in such cases, exhibit different viscosities and have vastly different surface energies. Viscous sintering kinetics are phenomenologically governed by the formation of the interphase due to droplet cohesion, the resultant phase equilibrium between coalescence and dispersion, and the subsequent densification of the intermingling polymer phases until air is excluded [16]. Idealised interparticle cohesion in the melt phase during rotomolding can be modeled by the evolution of two otherwise immiscible polymer particles melting adjacent to each other, undergoing bridging, and stabilising across the interfacial boundary as a single unified pool of liquid at the desired $PIAT$. Simply put, in order to improve dispersion and interparticle adhesion, we need to counter the coalescence of like particles and promote cohesion [17].

In this test, sintering behaviours of $HDPE$ and $PA11$ were observed via hot-stage microscopy, to evaluate the efficacy of 1 wt% surface-active agents Polybond 1009 (acrylic acid modified polyethylene), chitosan, or selected non-ionic surfactants (Pluronic F108, Span 60, Span 85, Tween 20, and Tween 60) in aiding interparticle adhesion. The purpose of the test was to narrow the surfactants for evaluation in the study down to only one or two species. The polymer particles were approximately 500 μm in Sauter mean diameter. As the lower melting temperature polymer, the surface-active agent was only applied to $HDPE$ particles. The $PA11$ was supplied with black pigmentation to aid in identifying the two phases during sintering. Surface active agents such as Polybond 1009 and chitosan,

which were insoluble in a carrier solvent, were placed in between the two adjacent $HDPE$ and $PA11$ particles. The efficacy of a surface-active agent in stabilising the "coalescence" or cohesion between $HDPE$ and $PA11$ particles was evaluated by the degree of contact at the interparticle boundary once reaching $PIAT$. Increased contact between the particles is reflective of a larger interphase region, and greater interfacial adhesion. Moreover, recall that there exists a third phase, the interphase, between the two polymer phases and miscibility is directly proportional to the thickness of the interphase. As the miscibility of the blend increases, the thickness of the interphase approaches infinity and the interfacial tension coefficient approaches zero [18]. Since the images captured via hot-stage microscopy are two-dimensional, favourable cohesion is represented by smaller overall areas of the two molten particles as observed via light microscopy (i.e. top-view). This is because an increase in the two-dimensional area across the plate surface suggests a decrease in height of the particle droplet in the z-direction (i.e. side-view), which means that the area in contact with the surroundings (i.e. air or the microscopy plate) is increasing, whereas the interfacial area between the two polymer particles is decreasing.

The sintering behaviour of $HDPE$ and $PA11$ particles without a surface-active agent coating is shown in Figure 4.4, where the nylon resin is dyed black to differentiate the particles. Figures 4.4a to 4.4b show the transition of both, $HDPE$ and $PA11$ resin particles from the solid phase to the melt phase. As the temperature increases to 215 °C in Figure 4.4c, the $HDPE$ particle distorts due to its innate

material properties and weak interfacial adhesion (i.e. low affinity) with the $PA11$ particle. Since we know that chemically similar particles are susceptible to coalescence, we can attribute the behaviour observed for $HDPE\text{-}PA11$ particle interactions to their relative immiscibility. This distortion of $HDPE$ is further exaggerated as the temperature increases and the interfacial region continues to decrease as the hot-stage reaches the desired rotomolding $PIAT$ of 235 °C.

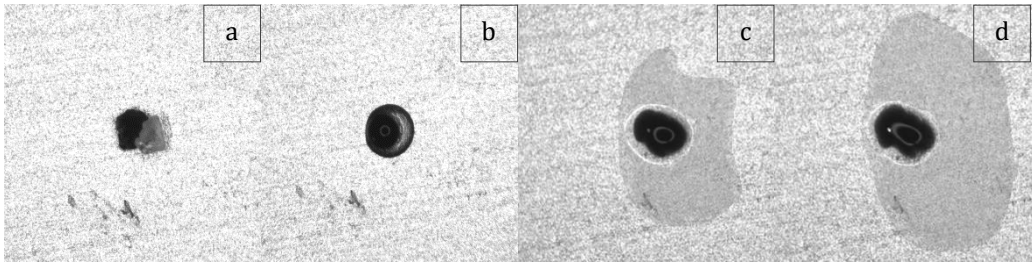

Figure 4.4. Interparticle cohesion of uncoated $HDPE\text{-}PA11$ at 25 °C [a], 195 °C [b], 215 °C [c], and 235 °C [d].

The behaviour of chitosan, Polybond 1009, and Pluronic F108 compatibilized sintered particles was similar to that of the uncoated particles. This can be attributed to two key factors: inadequate coating of $HDPE$ and unfavourable topology to grow the interphase. The non-ionic surfactants, such as sorbitan esters and their ethoxylated variants, however demonstrated favourable results as shown in Figures 4.5 and 4.6. Both Span 85 and Tween 20 are shown to successfully promote cohesion between $HDPE$ and $PA11$ particles as the temperature approached $PIAT$.

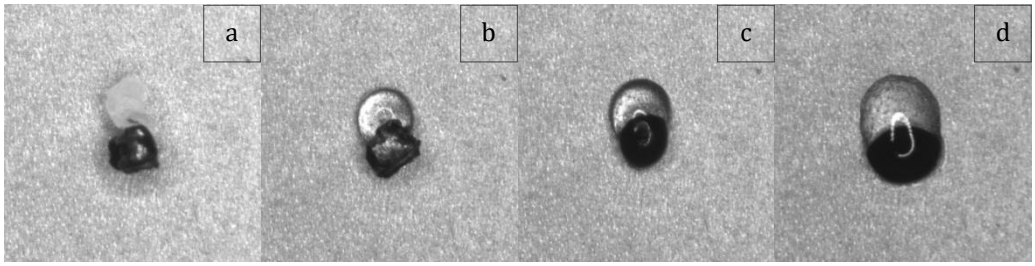

Figure 4.5. Interparticle cohesion of 1 wt% Span 85 coated $HDPE$-$PA11$ at 25 °C [a], 135 °C [b], 195 °C [c], and 235 °C [d].

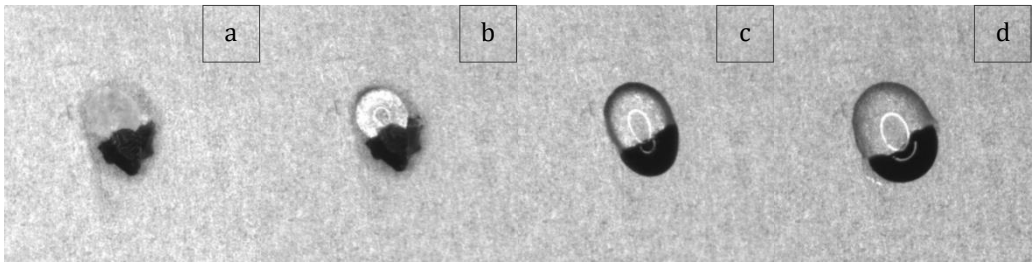

Figure 4.6. Interparticle cohesion of 1 wt% Tween 20 coated $HDPE$-$PA11$ at 25 °C [a], 135 °C [b], 195 °C [c], and 235 °C [d].

Literature explicitly investigating the utilization and incorporation of surface-active agents in rotomolded physical blends is scarce. Nevertheless, some categories of compatibilizers and surfactants have achieved varying degrees of success in blending immiscible polymers and preserving or enhancing their constituent properties in other processes. Since the role of compatibilizers in polymer blends may be understood to be identical to that of emulsifiers in classical emulsions [19], surfactants such as sorbitan esters and their ethoxylated variants were hypothesized to prove equally as effective in stabilising immiscible physical blends. This is because amphiphilic surfactants like Tween 20 have hydrophilic and lipophilic regions that can act as an adhesive and form intermolecular bonds with both $HDPE$ and $PA11$ polymer. Moreover, the hydrophilic-lipophilic balance

(HLB) of surfactants, whether high or low, is typically used as a preliminary metric to approximate the stabilisation of a colloidal suspension as either an oil-in-water or water-in-oil emulsion. In this case, use of Span 85 (HLB = 1.8) and Tween 20 (HLB = 16.7) may elicit melt-phase polymer migration of the constituent polymers in a predictable manner, resulting in $PA11$-in-$HDPE$ or $HDPE$-in-$PA11$ physical blends, respectively. Notwithstanding the relevance of the latter case in PFT applications (affording barrier properties against fossil fuels), both Tween 20 and Span 85, were investigated to test the polymer-migration hypothesis. However, the primary focus was Tween 20 since the expected resultant $HDPE$-in-$PA11$ blend theoretically meets the objective of forming a fuel-impermeable boundary around a structurally sound $HDPE$ wall.

4.4 Polymer Rheology and Zero-Shear Viscosity

Low apparent viscosity is preferred in rotomolding processes to facilitate favourable coalescence, densification, and overall sintering behaviour in general [20]. One of the effects of the surfactant on sintering and coalescence to be considered is plasticization, which aids the rotomolding process as mentioned above. Considering the optimal selected $PIAT$ for the rotomolding operations, which was determined to be 235 °C [13], the viscosities of the blend components with respect to surfactant concentration was explored, as shown in Figures 4.7 and 4.8 for $HDPE$ and $PA11$, respectively. The more representative viscosity for rotomolding is zero-shear viscosity, which in the present case was calculated using the Cross model and validated by the Carreau-Yasuda model.

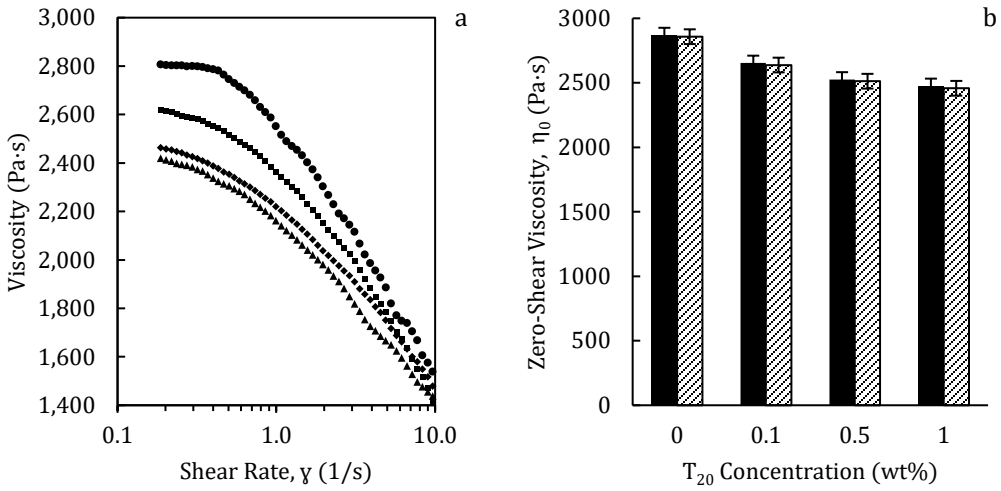

Figure 4.7. Viscosity-shear rate curves for uncoated (●), and 0.1% (■), 0.5% (◆), and 1.0% (▲) Tween 20 coated *HDPE* [a]; Cross (■) and Carreau-Yasuda (▨) zero-shear viscosities for concentrations of Tween 20 coated *HDPE* [b].

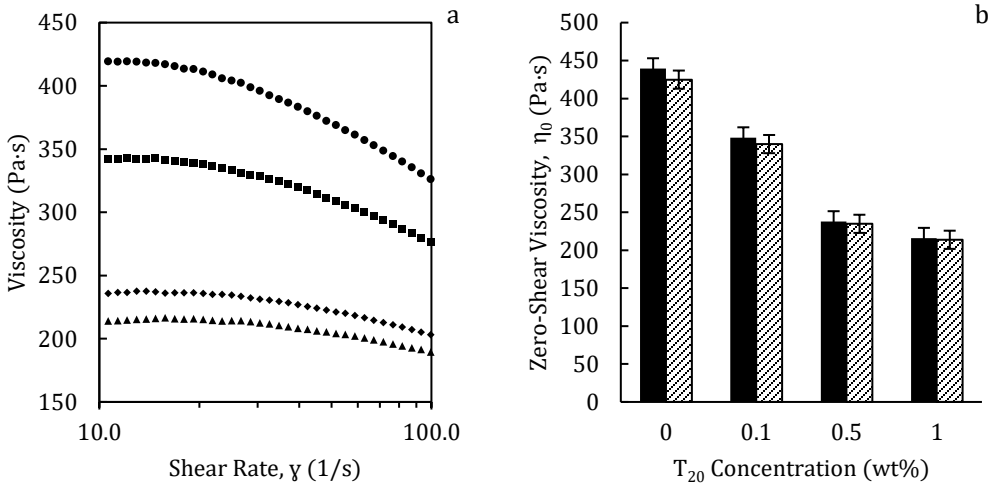

Figure 4.8. Viscosity-shear rate curves for uncoated (●), and 0.1% (■), 0.5% (◆), and 1.0% (▲) Tween 20 coated *PA*11 [a]; Cross (■) and Carreau-Yasuda (▨) zero-shear viscosities for concentrations of Tween 20 coated *PA*11 [b].

The zero-shear viscosity of *HDPE* decreased from 2689 Pa·s to 2475 Pa·s (8% decrease) with increasing Tween 20 concentration from 0 to 1 wt%, as shown

in Figure 4.7a. For $PA11$, an increase in surfactant concentration (0-1%) resulted in a proportionally greater decrease in viscosity from 439 Pa·s to 215 Pa·s (51% decrease). Even though the surfactant will only be applied to the $HDPE$ particles for rotomolding, we assume it remains at the boundary of the melt without diffusion into its interior during sintering and so, it is assumed the effects seen here are a valid representation of plasticization of both polymers at the interphase.

There are few examples in the literature where the rheological impact of a low molecular weight surfactant on a polymer melt are considered. However, the plasticization phenomenon observed for both polymers is consistent with the effects also observed for coatings of non-ionic surfactants, Alfonic 1412-3 ethoxylate and Aromox dimethylcocoalkylamine oxide on the viscosity of anionic polymer, Aqualon™ sodium carboxymethylcellulose [21]. Recall that the slip flow characteristics of the blend have an effect on the sintering mechanisms (i.e. coalescence and dispersion) in the zero-shear environment of a rotomolding process [22]–[25]. High melt viscosity has been shown to result in bubble formation and consequently poor mechanical properties [26]. Since the rate of coalescence increases as the viscosity of the blend components decrease, the reduction of viscosity due to the introduction of Tween 20 into the system is deemed particularly favourable. Therefore, Tween 20, which was shown to reduce the viscosity of the constituent polymers is likely to positively influence the melt-flow behaviour, phase dispersion, and sintering kinetics of the polymer components during rotomolding [1], [20].

4.4.1 Phase Inversion of Extrusion-Mixed Physical Blends

$HDPE$-$PA11$ polymer blends were investigated with an emphasis on retaining the functionality of $HDPE$ as the continuous matrix and $PA11$ as the secondary phase to contribute to the structural backbone and act as a barrier to fossil fuels in rotomolded articles, respectively. Since one of the objectives of this thesis is to explore avenues to form virtually indistinguishable fully co-continuous morphologies between the two otherwise immiscible phases (in addition to eliciting or predicting the migration of $HDPE$ and $PA11$ during mixing), it was worth determining whether or not the phase inversion point is possible, where the continuous matrix is indistinguishable from the dispersed phase, within the aforementioned boundaries of the project (i.e. concentration of $PA11 < 50\%$) [27]. To that end, the ratio between the viscosity of the dispersed and the continuous phases should ideally be close to unity, which results in the reduction of the interfacial tension, fosters dispersion, and improves miscibility, as defined by the phase viscosity ratio [28],

$$\lambda = \frac{\eta_{PA11}}{\eta_{HDPE}} \tag{4.2}$$

This is not possible for our system given that the zero-shear viscosities of $PA11$ are considerably lower than those of $HDPE$, as shown in Figures 4.7 and 4.8. However, the volume fractions of $HDPE$ required for full-continuity in $HDPE$-$PA11$ blends are 71% and 78% for concentrations of 0% and 1% Tween 20, respectively as estimated by,

$$\phi_{2,HDPE} = \frac{1 - \frac{\log \lambda}{[\eta]}}{2} \tag{4.3}$$

where, $\phi_{2,HDPE}$ is the volume fraction of $HDPE$, λ is the phase viscosity ratio, and η is the 'intrinsic viscosity' for phase inversion compositions with a reported value of 1.9 [29]. Therefore, although the phase viscosity ratio of the blend is unfavourable towards the objectives of this thesis, a fully co-continuous morphology is possible around the phase inversion concentration of 69 wt% and 76 wt% $HDPE$ for concentrations of 0% and 1% Tween 20, respectively within the defined parameters of this project.

4.5 Rotomolding Trials

4.5.1 Polymer Migration and Morphological Characterisation

Hydrophilic-lipophilic balance values are typically used to estimate oil-in-water or water-in-oil emulsions [30]. However, the practicality of that metric has not yet been explored for thermodynamically immiscible polymer blends where relatively hydrophobic and hydrophilic polymer may behave similarly in the melting and densification stages of a rotomolding cycle. Ideally, compatibilizing $HDPE$-$PA11$ blends using surfactants such as Tween 20 with a high HLB value should yield an oil-in-water or more appropriately a $HDPE$-in-$PA11$ phase morphology, whereas the opposite would hold true for surfactants with low HLB values, such as Span 85. This principle was investigated for both dry-mixed and melt-mixed blends, as shown in Figures 4.9, 4.10, and 4.11.

Figure 4.9 shows the phase dispersed morphology of $PA11$ in 50/50 blends after $HDPE$ was etched way from samples of the rotomolded wall cross-sections. Figures 4.9a to 4.9d represent the change in cross-section morphology as the concentration of Tween 20 increased. Although the results are by no means conclusive, it can be suggested that $PA11$ appeared to gradually migrate towards edge of the wall.

According to the crystallisation kinetics and the thermal behaviour observed for $HDPE$-$PA11$ blends (*see § 4.1*), $HDPE$ melts first, forming the matrix phase in which the $PA11$ resin was suspended until the temperature of the rotomolding heating cycle reaches the melting point of $PA11$, $T_{m_{PA11}}$. In 50/50 blends, upon melting, two possibilities exist: either $PA11$ droplets remain as the discrete phase and dispersed in the $HDPE$ continuous matrix or due to the onset of phase inversion, $PA11$ becomes the continuous phase and $HDPE$ transforms into the dispersed phase [31]. Recall that the phenomenon of the phase inversion concentration was explicitly associated with mechanically compatibilized blends and modeled as a function of the volume (or weight) fraction of the primary constituent polymers of the $HDPE$-$PA11$ polyblend (*see § 4.4.1*). From the observations for 50/50 dry-mixed rotomolded blends, we can posit that the phase inversion phenomenon is a function of surfactant concentration, whereby as the concentration of Tween 20 increased the blend reached a state wherein the dispersed phase transforms into the continuous phase and vice versa. Furthermore, the increase in surfactant concentration also resulted in an increase in the coalescence of chemically similar

particles. This behaviour can be attributed to simultaneous nucleation growth and spinodal decomposition resulting in phase separation across the miscibility boundary.

For the uncoated blend, as shown in Figure 4.9a, $PA11$ is dispersed more uniformly and present in relatively large quantities towards the center of the rotomolded wall cross-sections. Whereas, although the Span 85 compatibilized blend shows some degree of migration similar to Tween 20 compatibilized blends, a more detailed investigation is required over a range of Span 85 concentrations to draw any meaningful conclusions. Nevertheless, as shown in *§ 4.5.3*, Span 85 still shows an improvement in mechanical properties over the uncoated blends. As for the dry-mixed 75/25 blends, $PA11$ formed spherical droplets and remained as the dispersed phase in the $HDPE$ matrix, as shown in Figure 4.10. Moreover, there was no discernable difference between the uncoated and surfactant-compatibilized blends. Therefore, consolidating the results for both, 50/50 and 75/25 blends, we can suggest that the state of dispersion and the resultant phase morphology of dry-mixed rotomolded $HDPE$-$PA11$ blends was determined by the blend ratio *and* the concentration of the Tween 20 surfactant; a clear trend is observed for the migration of $PA11$ to the rotomolded wall surfaces as a function of increasing Tween 20 concentration for 50/50 blends, whereas no such trend was observed when increasing the polyblend ratio to 75/25.

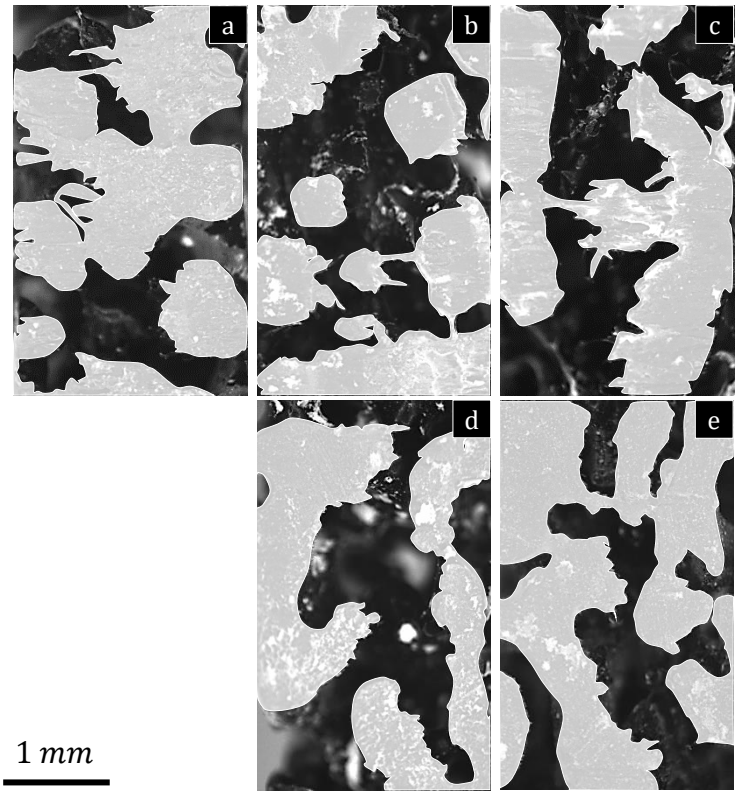

Figure 4.9. Microscopic morphologies of 50/50 $HDPE$ (unshaded) - $PA11$ (shaded) rotomolded physical blends with no surfactant [a], 0.1 wt% Tween 20 [b], 0.5 wt% Tween 20 [c], 1.0 wt% Tween 20 [d], and 1.0 wt% Span 85 [e].

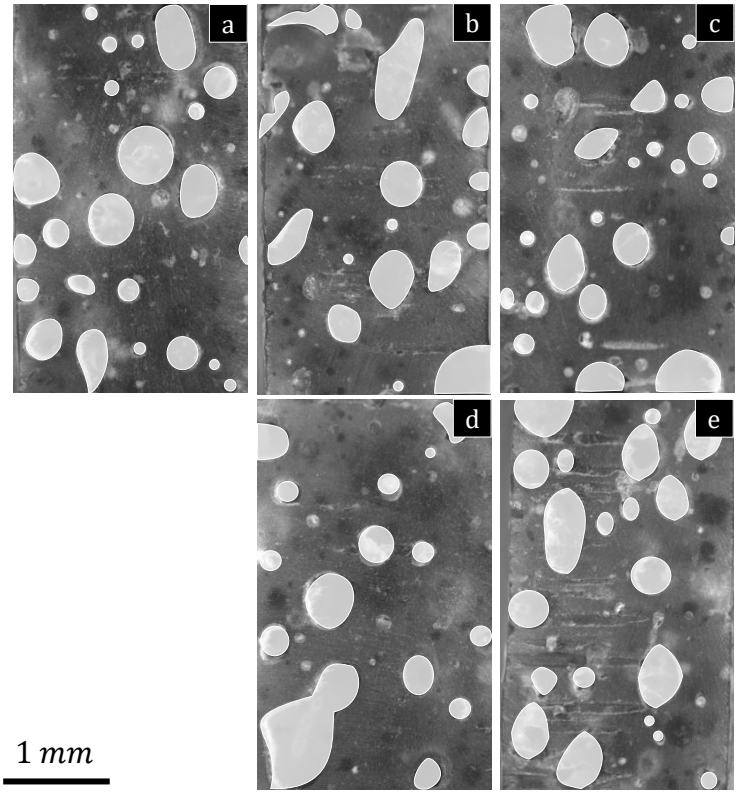

Figure 4.10. Microscopic morphologies of 75/25 $HDPE$ (unshaded) - $PA11$ (shaded) rotomolded physical blends with no surfactant [a], 0.1 wt% Tween 20 [b], 0.5 wt% Tween 20 [c], 1.0 wt% Tween 20 [d], and 1.0 wt% Span 85 [e].

Conversely, the phase morphology of extrusion-mixed blends is driven by the viscosity ratio, as shown in Figure 4.11, where once again an etchant was used to etch away regions of $HDPE$ of a sample from a rotomolded part, leaving behind $PA11$. This voidage as highlighted in the images is a representation of $HDPE$ regions of the rotomolded blend. In this case, we observe flow-induced encapsulation of $HDPE$ particles. Simply put, since $HDPE$ had a higher viscosity compared to $PA11$, the morphologies observed for these extrusion-mixed samples are consistent with a trend observed in polymer processing methods, whereby low

viscosity components will migrate towards the high stress regions and encapsulate the high viscosity component within [32].

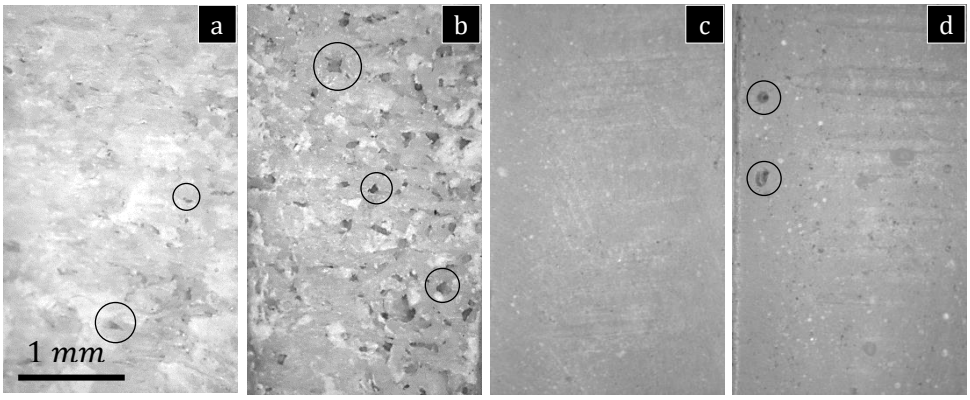

Figure 4.11. Microscopic morphologies of extrusion-blended 50/50 $HDPE$-$PA11$ with no surfactant [a] and 0.1 wt% Tween 20 [b]; and 75/25 $HDPE$-$PA11$ with surfactant [c] and 0.1 wt% Tween 20 [d] rotomolded physical blends; $HDPE$ is etched away (i.e. visually represented as voidage, select regions of $HDPE$ are highlighted).

Alternatively, we can explain the morphological differences by the phase inversion phenomenon discussed in *§ 4.4.1*, where the dispersed phase (i.e. $PA11$) was expected to transform into the continuous phase at approximately 75 wt% $HDPE$ and full co-continuity rendered both phases virtually indistinguishable from each other. As such, whereas regions of $HDPE$ were etched away in the 50/50 blend, the 75/25 blend is practically unaffected. Lastly, the presence of Tween 20 in extrusion-mixed blends appeared to have an adverse effect resulting in increased voidage for both 50/50 and 75/25 blends. These observations and explanations are based on the assumptions that the theory of melt-memory in polymer crystallisation holds true [33]. That is, the ground extrudate when rotomolded exhibits identical crystallisation behaviour to when the blend was first processed via extrusion-

mixing. Any changes in the phase dispersion morphology during the reprocessing and re-crystallization of the ground extrudate via rotomolding are negligible.

4.5.2 Density and Porosity

In lieu of long-term penetrant permeability and diffusivity studies, measurements for density and porosity of the polymer matrix were conducted to characterise its barrier properties and the mass transfer tortuous diffusion pathways of the rotomolded $HDPE\text{-}PA11$ blends. Furthermore, an increase in density or alternatively, a decrease in porosity, for the sintered mass is often correlated with an improvement in material properties, such as impact strengths and flexural moduli [34]. Density values for the 50/50 $HDPE\text{-}PA11$ blends are given in Figure 4.12. Both density and porosity measurements communicate the same trend in densification behaviour, however the latter characterisation accounts for the effect of blend ratio and allows for better visualisation of the influence of surfactants on the blends' resultant material properties. As such, the porosity values for 50/50 $HDPE\text{-}PA11$ blends are given in Figure 4.13. Porosity was calculated using equation (3.5) in *§ 3.3.1*.

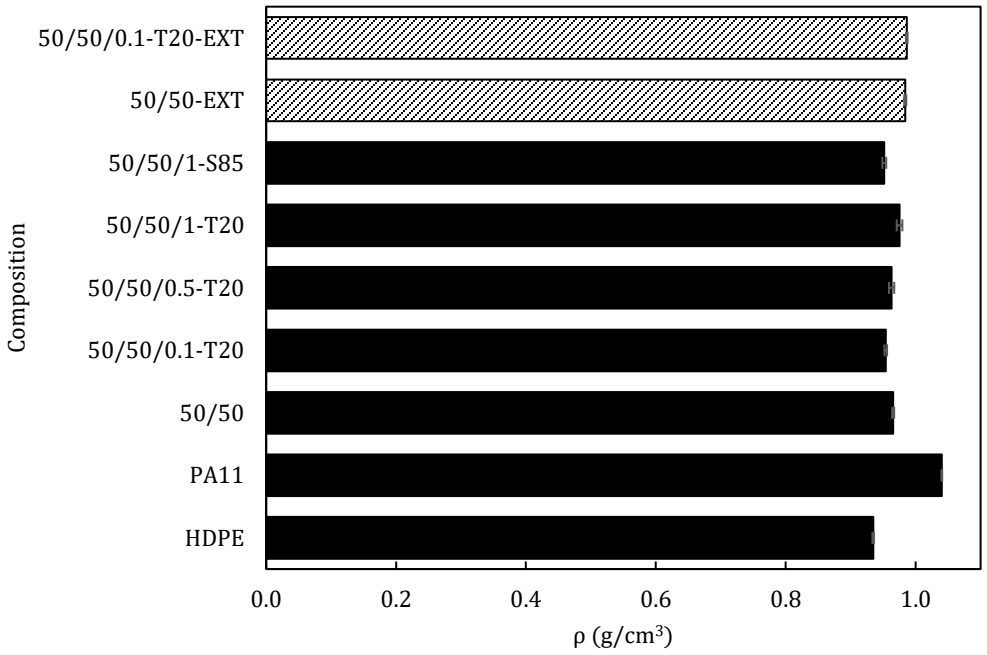

Figure 4.12. Densities of 50/50 $HDPE\text{-}PA11$ rotomolded (■) and pre-extruded rotomolded (▨) blends.

The introduction of Tween 20 has a negative effect on the density/porosity of rotomolded 50/50 $HDPE\text{-}PA11$ blends up to a surfactant concentration of 0.5 wt%, after which porosity decreases by 31.17% for a Tween 20 concentration of 1.0 wt%, compared to the uncoated blend. At low concentrations, the presence of Tween 20 may be inhibiting interparticle cohesion and coalescence. Recall that *cohesion* refers to the unification of immiscible particles, whereas *coalescence* is used to describe the flocculation of like particles. This can adversely affect the sintering kinetics of the polyblend system, resulting in the evolution of air bubbles, consequent bubble formation during densification, and poor stabilisation [35]. Whereas the improvement at 1 wt% Tween 20 may be attributed to actual thickening of the interphase region. At higher concentrations of Tween 20, the

improvement in melt-flow due to lower viscosities compensates for the increase in the viscosity ratio, leading to improved mixing, yielding flow-induced coalescence, and an increase in compatibilizer-localised regions of miscibility. The onset of these favourable phenomena result in an increase in interfacial adhesion and better phase dispersion morphology.

In the case of rotomolded parts prepared with the extrusion-mixed blend, its uncoated and 0.1 wt% Tween 20 coated blends show a 59% and 66% improvement over dry-blended uncoated blends, respectively. The drastic improvement in density and porosity is consistent with polymer blends processed via extrusion, wherein increased interfacial adhesion and phase dispersion due to mechanical compatibilization compensates for the introduction of mechano-chemical and thermo-oxidative degradation [36], [32]. Recall, that this explanation and all discussions regarding extrusion-mixed rotomolded blends herein, is under the premise that the second recrystallisation of such $HDPE\text{-}PA11$ blends depends on its melt-phase behaviour during extrusion [33].

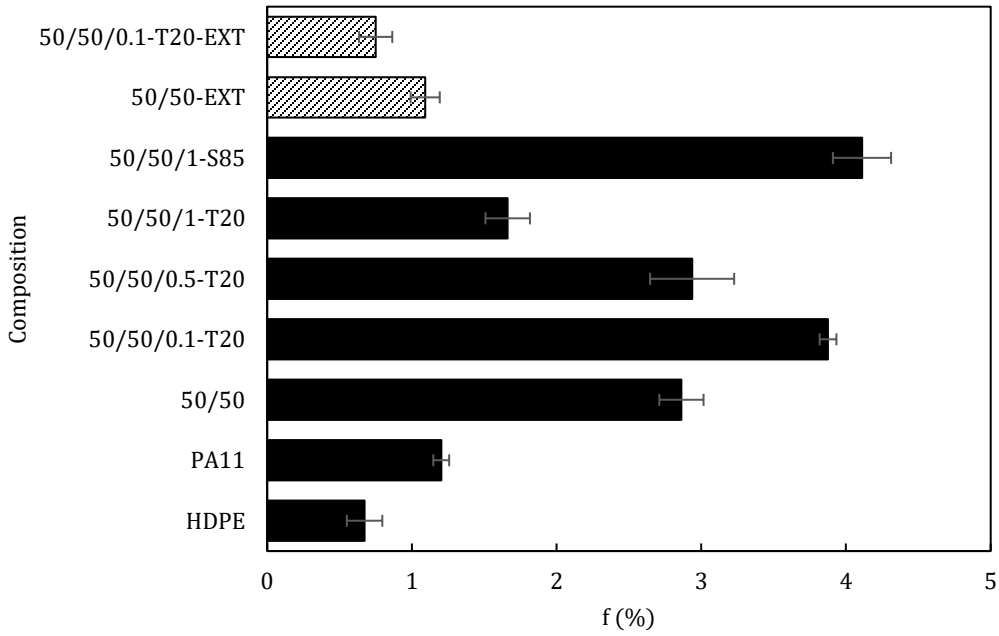

Figure 4.13. Porosities of 50/50 $HDPE$-$PA11$ rotomolded (■) and pre-extruded rotomolded (▨) blends.

Conversely, the introduction of Span 85 at 1 wt% resulted in an increase in porosity by 39% compared to the uncoated 50/50 dry-mixed blend. This behaviour is also observed for the 75/25 $HDPE$-$PA11$ blends, where using the density values from Figure 4.14, the porosity of 1 wt% Span 85 coated blends as shown in Figure 4.15, was determined to increase by 28% compared to the uncoated blend. The utility of introducing surfactants into a polyblend system is gauged on its ability to provide localised regions of miscibility, which promote interfacial adhesion, and simultaneous interparticle cohesion and coalescence of the constituent polymers [37], [38]. To that end, analysing the chemical structure of Tween 20 and Span 85 may provide essential insight into why the surfactants yield drastically different results at a concentration of 1 wt% in $HDPE$-$PA11$ blends.

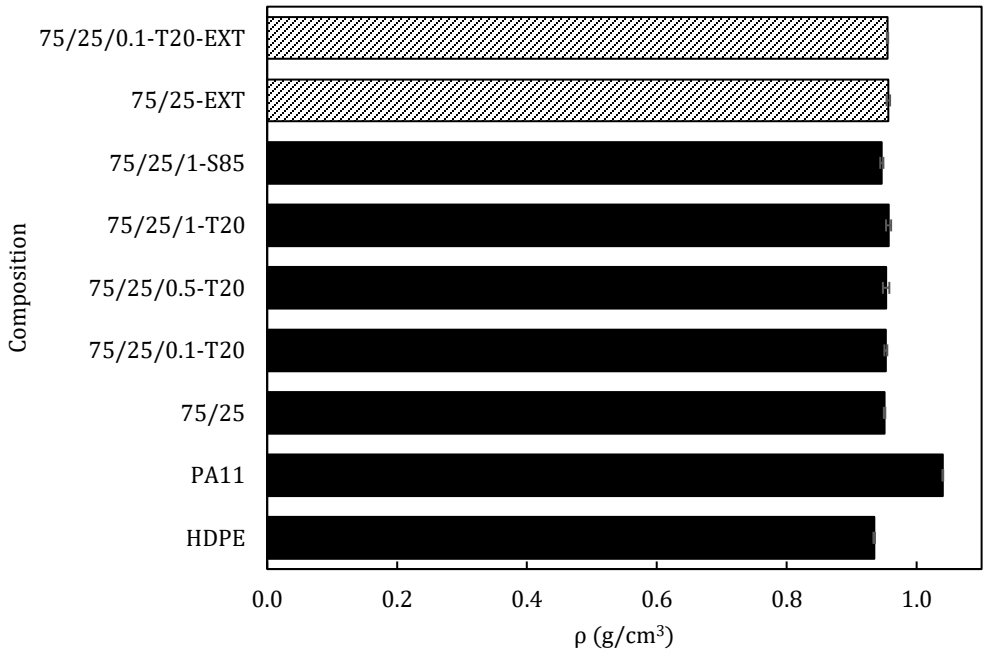

Figure 4.14. Densities of 75/25 $HDPE\text{-}PA11$ rotomolded (■) and pre-extruded rotomolded (▨) blends.

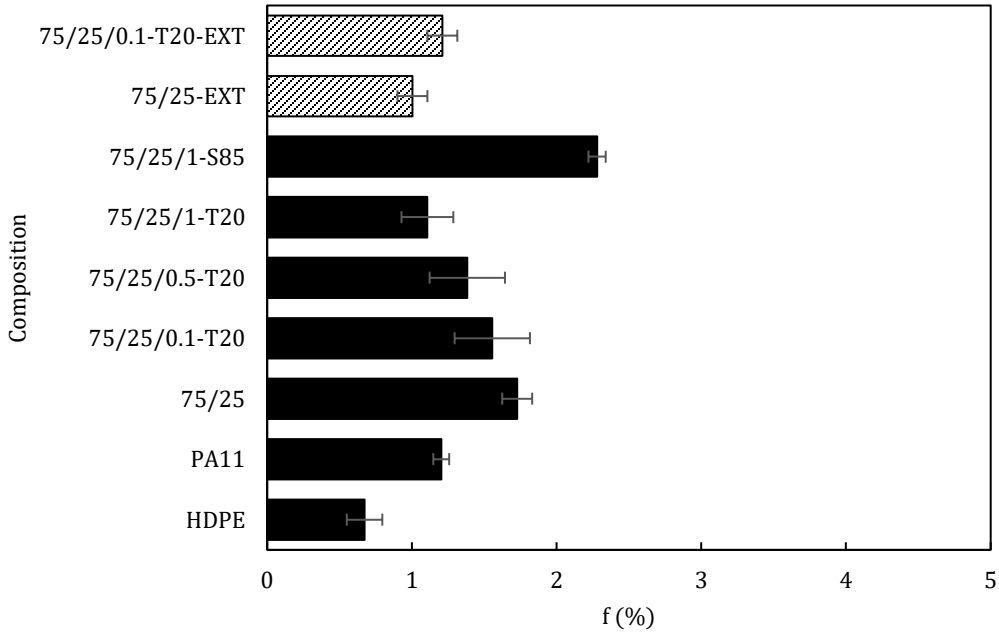

Figure 4.15. Porosities of 75/25 $HDPE\text{-}PA11$ rotomolded (■) and pre-extruded rotomolded (▨) blends.

The topology of non-ionic surfactants such as Tween 20 and Span 85 must have hydrophilic and lipophilic regions, which have accessible and stable sites for hydrogen-bonding with chains of $PA11$ and Van der Waals bonding with chains of $HDPE$, respectively. $PA11$ has two sites for hydrogen-bonding, one of which behaves as a proton acceptor and the other as a proton donor, whereas $HDPE$ bonds along the length of its hydrocarbon backbone via Van der Waals forces. Span 85, as shown in Figure 4.16 has six sites for hydrogen bonding which act as proton acceptors, two which act as proton donors, and three oleophilic branches [35].

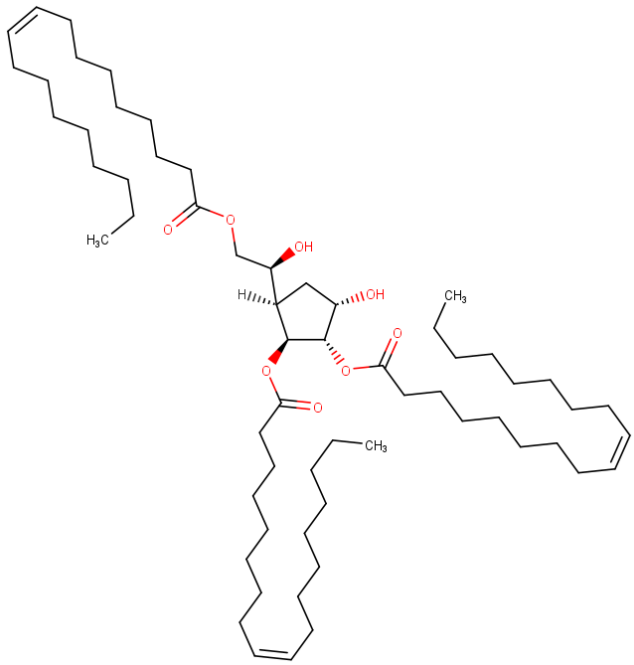

Figure 4.16. Chemical structure of sorbitan trioleate (Span 85).

Whereas, Tween 20 has one oleophilic branch, three sites which act as proton donors, and 23 sites that act as proton acceptors, of which 20 are distributed across the four repeating units, *w*, *x*, *y*, and *z* of polyethylene glycol. Compared to Span

85, Tween 20 has a more saturated hydrophilic region, which has both hydrogen bond acceptor and donor sites that are more accessible to bond with $PA11$. Although Span 85 has a greater number of oleophilic branches, its hydrophilic region is relatively less accessible whereby potential bonding with $PA11$ is less likely, since $PA11$ chains are more prone to repulsion from the hydrophilic region of Span 85 due to steric effects. Furthermore, at 1.0 wt% concentration of Span 85, the surfactant may have exceeded its critical micelle concentration which has been shown to facilitate macroscopic phase separation [39].

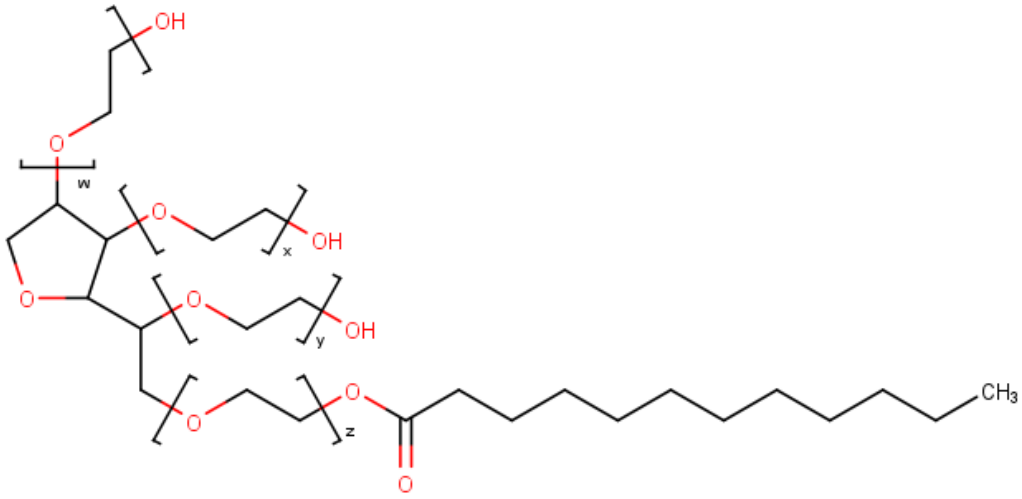

Figure 4.17. Chemical structure of polyoxyethylene sorbitan monolaurate (Tween 20).

However, Span 85 cannot be assumed to further exacerbate the instability by interfering with intermolecular interactions resulting in less regular packing of chains of $HDPE$. As shown in *§ 4.5.3*, the mechanical properties for blends compatibilized using 1 wt% Span 85 are either on par or marginally better than those blended with 1 wt% Tween 20. This means that Span 85 in $HDPE$-$PA11$

blends has potentially stronger but fewer overall bonds with its constituent components. As such, Span 85 likely favours bonding with $HDPE$ over $PA11$ because of its three oleophilic branches, therefore yielding rotomolded parts that are less dense but equally as strong as those compatibilized using Tween 20.

As for the comparison between 75/25 dry-mixed blends compatibilized using different concentrations of Tween 20, these blends exhibit a similar trend to the 50/50 blends in that porosity decreased with increasing surfactant concentration. However, compared to the 50/50 blends, the use of Tween 20 showed an improvement over uncoated blends for all concentrations of the surfactant. At low concentrations, Tween 20 can simply hinder both interparticle cohesion and coalescence in a 50/50 blend. As the concentration of Tween 20 or $HDPE$ increases, the likelihood of interactions between Tween 20 and $HDPE$ increases, resulting in an overall increase in density and decrease in porosity.

4.5.3 Impact and Flexural Properties

The results in this section for impact and flexural strength are given as specific properties using density as the intrinsic property of the rotomolded blends (see equation (3.7) and (3.9) in *§ 3.3.5* and *§ 3.3.6*, respectively) to normalize the results relative to porosity and therefore, focus on the interfacial effects of adding a surfactant into the process. Two general trends were observed while characterising the mechanical properties of rotomolded samples for both 50/50 and 75/25 dry-mixed and extrusion-mixed $HDPE$-$PA11$ blends.

The impact strengths for all surfactant-compatibilized dry-mixed parts increased as a function of Tween 20 concentration. Conversely, the impact strength decreased for extrusion-mixed blends compared to dry-mixed blends and the introduction of 0.1 wt% Tween 20 into the polyblend system yielded negligible results. The specific impact strengths for 50/50 and 75/25 blends are given in Figures 4.18 and 4.19, respectively. Secondly, although the introduction of Tween 20 into a 75/25 polyblend system yielded a similar trend in the improvement of specific flexural strengths, the effect of changing the mixing strategy from dry-mixed to extrusion-mixed produced the opposite effect in both 50/50 and 75/25 blends, as shown in Figures 4.20 and 4.21 respectively, with the latter proving to be more favourable.

It is not uncommon for dry-mixed and extrusion-mixed rotomolded elements to demonstrate drastically different and inverse effects on mechanical and tensile properties depending on the mixing strategy. This behaviour was also observed to be the case for rotomolded blends of poly(lactic acid) and linear medium density polyethylene, where different mixing strategies at any given weight ratio produced drastically different results [40], [41]. Similar to *§ 4.5.2*, the discussion in this section will be broken into three parts:

1. The effect of Tween 20 concentration, volume fraction of $HDPE$, and mixing strategy on the specific impact strength of rotomolded blends.
2. Comparing trends for specific impact strengths and specific flexural strengths.

3. The effect of Tween 20 concentration, volume fraction of $HDPE$, and mixing strategy on the specific flexural strength of rotomolded blends.

The improvement in mechanical properties is understandably expected of homogeneous, thermodynamically miscible blends. In cases of miscible polymer blends, composite properties occasionally exceed the principle of additivity based on the individual properties of the constituent blends as observed for polystyrene – poly-2,6-dimethyl-1,4-phenyleneether blends [42]. Similarly, immiscible polymer blends of polyethylene terephthalate and polycarbonate demonstrated exceptionally enhanced impact properties when compatibilized with styrene-acrylonitrile grafted ethylene propylene diene monomer ($EPDM$) copolymers [43].

In addition to miscible polymer blends and those compatibilized using especially tailored co-polymers, the elevation of mechanical and tensile properties is also possible for surfactant-compatibilized blends. Isotactic polypropylene (PP) and calcium carbonate ($CaCO_3$) nanocomposites showed a significant increase in impact properties, where concentrations of non-ionic polyoxyethylene nonylphenol < 2.25% drastically improved the dispersion of $CaCO_3$ in the PP matrix [44]. Furthermore, incorporating small amounts of ionic liquid-based surfactants and non-ionic surfactants yielded improved tensile properties for polybutylene succinate – rice starch and high-density polyethylene – low-density polyethylene – cellulose blends, respectively [45], [46].

Similarly, as mentioned above, the impact strengths for all surfactant-compatibilized dry-mixed blends increased compared to the uncoated blends, with

the values peaking at 0.5 wt% Tween 20 concentration for both 50/50 and 75/25 blend ratios. Recall that when a surfactant exceeds its critical micelle concentration, a polyblend can undergo macroscopic phase separation [39]. The resultant self-aggregation of the surfactant molecules can act as an impurity that further exacerbates the immiscibility of the system by inhibiting interparticle cohesion and coalescence. The overall improvement for both Tween 20 and Span 85 compatibilized blends is expected as explained in the discussion regarding their topology in *§ 4.5.2*. At 1 wt%, both Tween 20 and Span 85 provide high concentrations of hydrophilic and lipophilic regions for $PA11$ and $HDPE$ to interact with, respectively.

Lastly, the difference between uncoated and 0.1 wt% Tween coated extrusion-mixed blends is negligible. The overall degradation in the specific impact strength for extrusion-mixed blends compared to dry-mixed blends can be explained as a consequence of exposing the blend to high stresses during extrusion, which resulted in regions of higher crystallinity and higher residual stresses. Furthermore, the extrusion process exposes the material to mechano-chemical degradation in addition to potential thermo-oxidative degradation, both of which can result in a deterioration of the blends' mechanical properties.

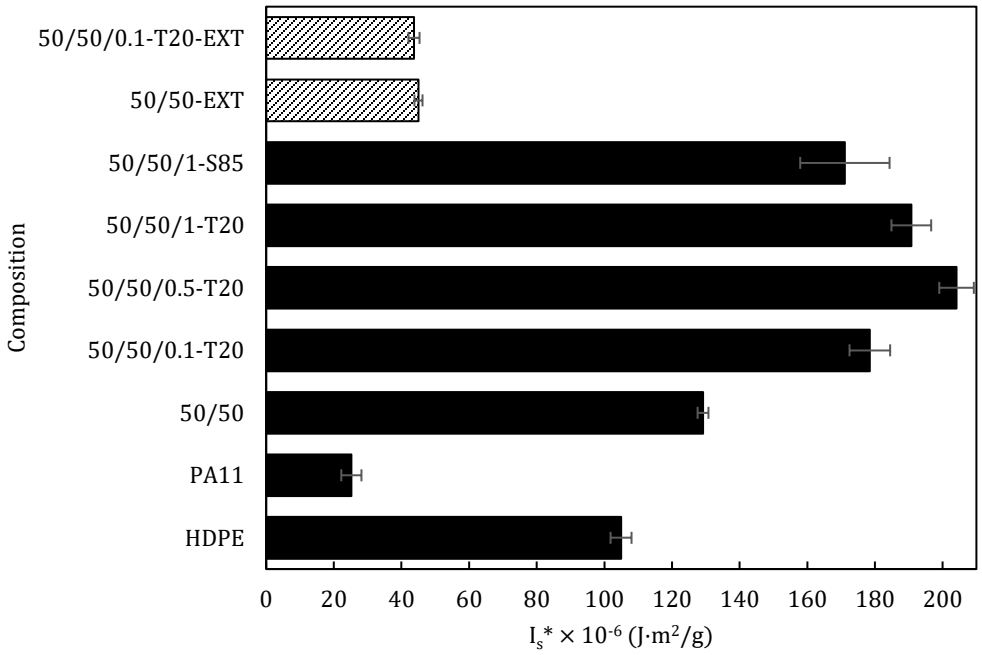

Figure 4.18. Specific impact strengths of 50/50 $HDPE$-$PA11$ rotomolded (■) and pre-extruded rotomolded (▨) blends.

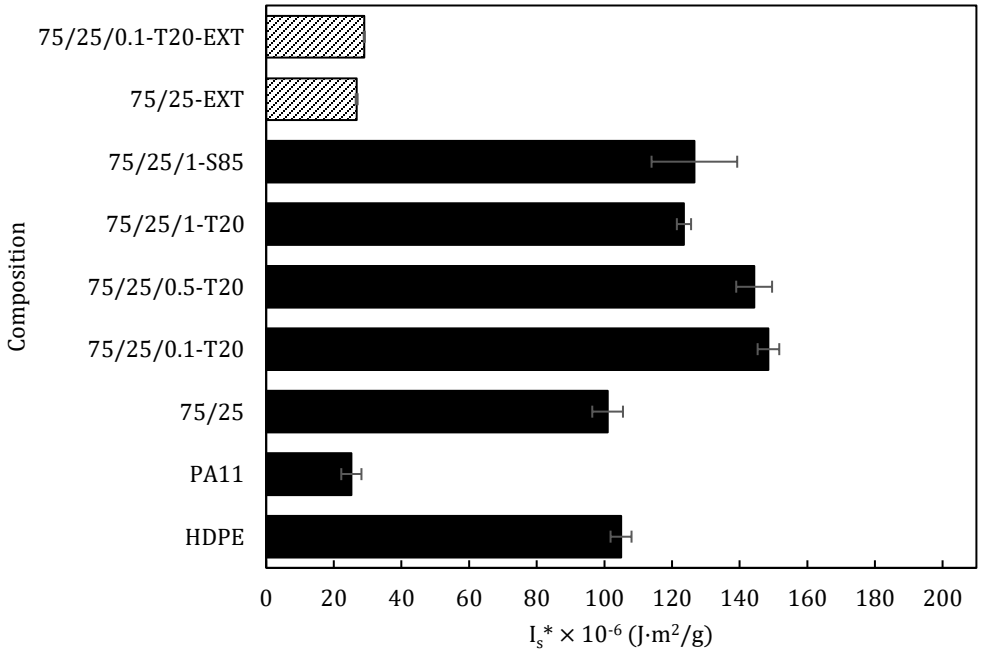

Figure 4.19. Specific impact strengths of 75/25 $HDPE$-$PA11$ rotomolded (■) and pre-extruded rotomolded (▨) blends.

With regards to flexural strength, it is important to note that high- (i.e. impact strength) and low-speed (i.e. flexural strength) characterisation techniques measure independent intrinsic properties of materials. That is, an improvement in a material's impact strength does not necessarily reflect an improvement in its flexural strength or vice versa. That being said, it is evident from Figures 4.20 and 4.21 that chemical compatibilization using Tween 20 has an adverse effect on the specific flexural strength of dry-mixed $HDPE\text{-}PA11$ blends, whereas incorporating mechanical compatibilization (i.e. extrusion-mixing) improves it. As for the effect of introducing Tween 20 to the extrusion-mixed blend, the dataset is too limited to make any conclusive assessments.

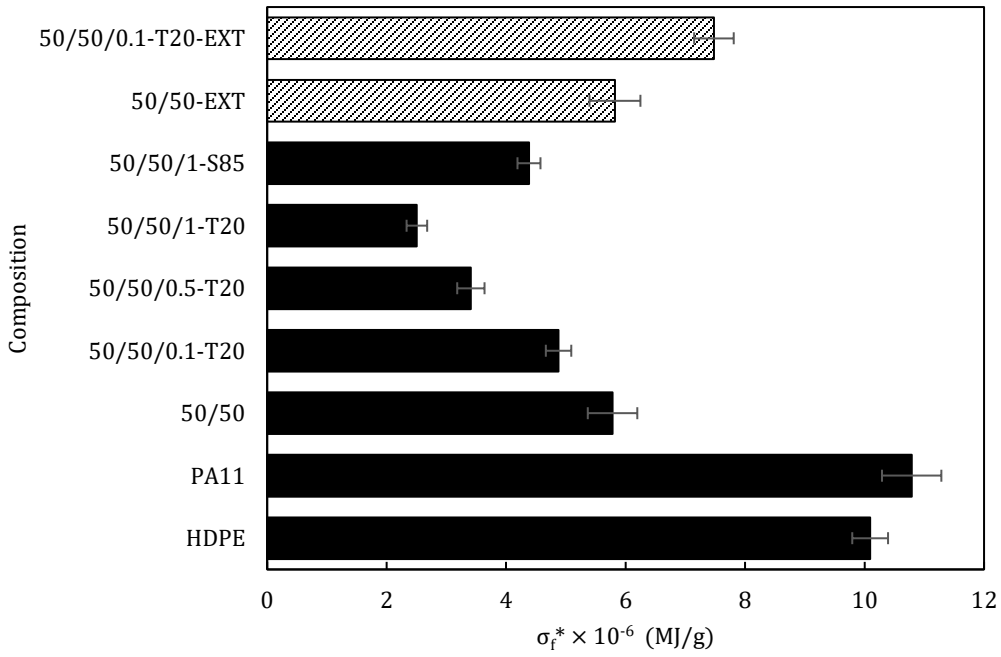

Figure 4.20. Specific flexural strengths at 5% strain of 50/50 $HDPE\text{-}PA11$ rotomolded (■) and pre-extruded rotomolded (▨) blends.

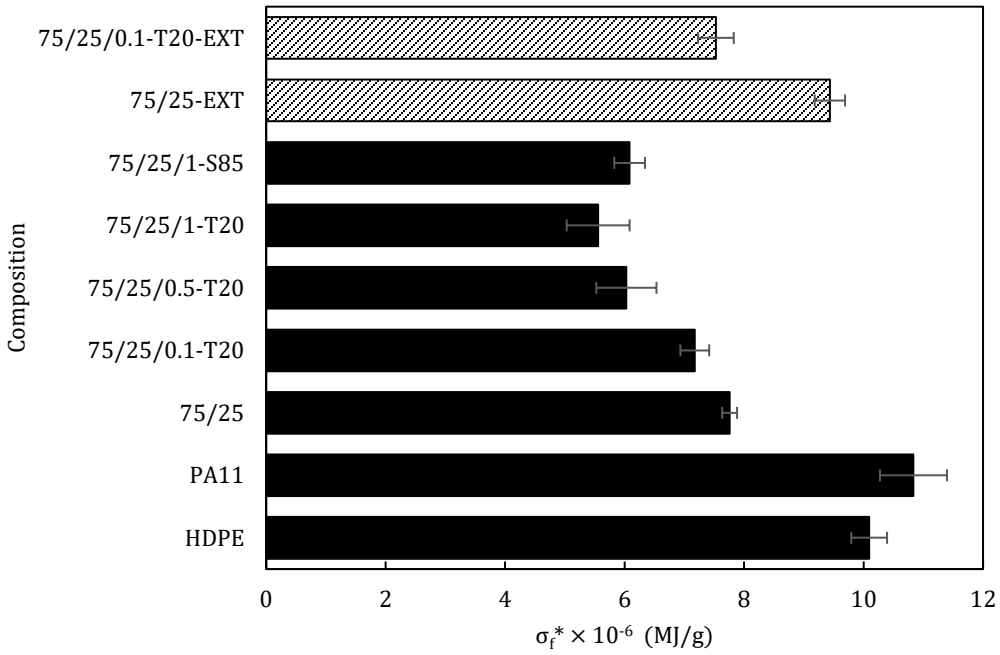

Figure 4.21. Specific flexural strengths at 5% strain of 75/25 $HDPE$-$PA11$ rotomolded (■) and pre-extruded rotomolded (▨) blends.

Overall, it is clear that increasing the mass fraction of $HDPE$ in the polyblend resulted in an improvement of the blends' flexural strengths. Therefore, based on the observations for both impact and flexural strengths, we can conclude that the ideal combination of mixing strategy, Tween 20 concentration, and blend ratio depends on the specific-use case scenario for which the $HDPE$-$PA11$ rotomolded blends is designed for.

4.6 References

[1] S. Jabarin, K. Majdzadeh-Ardakani and E. Lofgren, "Crystallization and Melting Behavior in Polymer Blends," *Encyclopedia of Polymer Blends*, pp. 135-190, 2016. Available: 10.1002/9783527653966.ch2.

[2] G. Groeninckx, M. Vanneste and V. Everaert, "Crystallization, Morphological Structure, and Melting of Polymer Blends," *Polymer Blends Handbook*, pp. 203-294, 2003. Available: 10.1007/0-306-48244-4_3.

[3] A. Shultz and A. Young, "DSC on Freeze-Dried Poly(methyl methacrylate)-Polystyrene Blends," *Macromolecules*, vol. 13, no. 3, pp. 663-668, 1980. Available: 10.1021/ma60075a034.

[4] TN048, "Polymer Heats of Fusion", TA Instruments, New Castle, DE.

[5] H. Brown, K. Char and V. Deline, "Block Copolymers and Adhesion Between Immiscible Polymers," *Integration of Fundamental Polymer Science and Technology—5*, pp. 51-60, 1991. Available: 10.1007/978-94-011-3890-1_6.

[6] Z. Bartczak and A. Galeski, "Homogeneous nucleation in polypropylene and its blends by small-angle light scattering," *Polymer*, vol. 31, no. 11, pp. 2027-2038, 1990. Available: 10.1016/0032-3861(90)90072-7.

[7] C. Chen, E. Fontan, K. Min and J. White, "An investigation of instability of phase morphology of blends of nylons with polyethylenes and polystyrenes and effects of compatibilizing agents," *Polymer Engineering and Science*, vol. 28, no. 2, pp. 69-80, 1988. Available: 10.1002/pen.760280203.

[8] G. Groeninckx, C. Harrats, M. Vanneste, and V. Everaert, "Crystallization, Micro- and Nano-structure, and Melting Behavior of Polymer Blends," in *Polymer Blends Handbook*, L. A. Utracki and C. A. Wilke, Eds. 2nd ed., Dordrecht: Springer Netherlands, 2014, ch. 3, pp. 291-446.

[9] N. Rozik, A. Khalaf and A. Ward, "Studies the behaviors of polyaniline on the properties of PS/PMMA blends," *Proceedings of the Institution of Mechanical Engineers, Part L: Journal of Materials: Design and*

Applications, vol. 230, no. 2, pp. 526-536, 2015. Available: 10.1177/1464420715581196.

[10] M. R. Kamal, L. A. Utracki, and A. Mirzadeh, "Rheology of Polymer Alloys and Blends," in *Polymer Blends Handbook*, L. A. Utracki and C. A. Wilke, Eds. 2nd ed., Dordrecht: Springer Netherlands, 2014, ch. 7, pp. 725-874.

[11] M. Cramez, M. Oliveira and R. Crawford, "Optimisation of rotational moulding of polyethylene by predicting antioxidant consumption," Polymer Degradation and Stability, vol. 75, no. 2, pp. 321-327, 2002. Available: 10.1016/s0141-3910(01)00234-8.

[12] K. Ogila, M. Shao, W. Yang and J. Tan, "Rotational molding: A review of the models and materials," Express Polymer Letters, vol. 11, no. 10, pp. 778-798, 2017. Available: 10.3144/expresspolymlett.2017.75.

[13] X. Colin and J. Verdu, "Polymer degradation during processing," *Comptes Rendus Chimie*, vol. 9, no. 11-12, pp. 1380-1395, 2006. Available: 10.1016/j.crci.2006.06.004.

[14] M. Oliveira, M. Cramez and R. Crawford, "Structure-properties relationships in rotationally moulded polyethylene," Journal of Materials Science, vol. 31, no. 9, pp. 2227-2240, 1996. Available: 10.1007/bf01152932.

[15] M. Asgarpour, F. Bakir, S. Khelladi, A. Khavandi and A. Tcharkhtchi, "3D model for powder compact densification in rotational molding," *Polymer Engineering & Science*, vol. 52, no. 9, pp. 2033-2040, 2012. Available: 10.1002/pen.23133.

[16] A. Hamidi et al., "Modelling of sintering during rotational moulding of the thermoplastic polymers," *International Journal of Material Forming*, vol. 9, no. 4, pp. 519-530, 2015. Available: 10.1007/s12289-015-1239-6.

[17] L. Djaković, P. Dokić, P. Radivojević, I. Šefer and V. Sovilj, "Action of emulsifiers during homogenization of o/w emulsions," *Colloid & Polymer Science*, vol. 265, no. 11, pp. 993-1000, 1987. Available: 10.1007/bf01412403.

[18] L. A. Utracki, G. Z.-H. Shi, D. Rodrigue, and R. Gonzalez-Núñez, "Compounding Polymer Blends," in *Polymer Blends Handbook*, L. A. Utracki and C. A. Wilke, Eds. 2nd ed., Dordrecht: Springer Netherlands, 2014, ch. 9, pp. 919-1028.

[19] L. Utracki, *Polymer alloys and blends*. Munich: Hanser, 1990.

[20] M. Kontopoulou and J. Vlachopoulos, "Bubble dissolution in molten polymers and its role in rotational molding," *Polymer Engineering & Science*, vol. 39, no. 7, pp. 1189-1198, 1999. Available: 10.1002/pen.11505.

[21] J. Cailloux et al., "Effect of the viscosity ratio on the PLA/PA10.10 bioblends morphology and mechanical properties," *Express Polymer Letters*, vol. 12, no. 6, pp. 569-582, 2018. Available: 10.3144/expresspolymlett.2018.47.

[22] M. Rao and J. Throne, "Principles of rotational molding," *Polymer Engineering and Science*, vol. 12, no. 4, pp. 237-264, 1972. Available: 10.1002/pen.760120402.

[23] C. Bellehumeur, M. Kontopoulou and J. Vlachopoulos, "The role of viscoelasticity in polymer sintering," *Rheologica Acta*, vol. 37, no. 3, pp. 270-278, 1998. Available: 10.1007/s003970050114.

[24] J. Olinek, C. Anand and C. Bellehumeur, "Experimental study on the flow and deposition of powder particles in rotational molding," *Polymer Engineering & Science*, vol. 45, no. 1, pp. 62-73, 2004. Available: 10.1002/pen.20230.

[25] A. Greco and A. Maffezzoli, "Powder-shape analysis and sintering behavior of high-density polyethylene powders for rotational molding," *Journal of Applied Polymer Science*, vol. 92, no. 1, pp. 449-460, 2004. Available: 10.1002/app.20012.

[26] P. Y. Kelly, "A microscopic examination of rotomoulded polyethylene," *DuPont*, Toronto, Canada, 1981.

[27] F. Prochazka, M. Castro, C. Celle and C. Carrot, "Phase Inversion and Cocontinuity in Immiscible Polymer Blends," in 37ème Colloque annuel du Groupe Français de Rhéologie, Saint-Etienne, Nov. 2012.

[28] J. Cailloux et al., “Effect of the viscosity ratio on the PLA/PA10.10 bioblends morphology and mechanical properties,” *Express Polymer Letters*, vol. 12, no. 6, pp. 569-582, 2018. Available: 10.3144/expresspolymlett.2018.47.

[29] L. Utracki, “On the viscosity-concentration dependence of immiscible polymer blends,” Journal of Rheology, vol. 35, no. 8, pp. 1615-1637, 1991. Available: 10.1122/1.550248.

[30] E. Martins, D. Renard, Z. Adiwijaya, E. Karaoglan and D. Poncelet, “Oil encapsulation in core–shell alginate capsules by inverse gelation. I: dripping methodology,” *Journal of Microencapsulation*, vol. 34, no. 1, pp. 82-90, 2017. Available: 10.1080/02652048.2017.1284278.

[31] J. Lee and C. Han, "Evolution of polymer blend morphology during compounding in an internal mixer", *Polymer*, vol. 40, no. 23, pp. 6277-6296, 1999. Available: 10.1016/s0032-3861(99)00022-1.

[32] L. A. Utracki, “The Rheology of Multiphase Systems,” in *Rheological Fundamentals of Polymer Processing*, J. Covas, J. Agassant, A. Diogo and J. Vlachopoulos, Eds. Dordrecht: Springer Netherlands, 2010, pp.113-137.

[33] M. Muthukumar, "Communication: Theory of melt-memory in polymer crystallization", *The Journal of Chemical Physics*, vol. 145, no. 3, p. 031105, 2016. Available: 10.1063/1.4959583.

[34] I. Hong, S. Kim and S. Lee, “Effects of HLB value on oil-in-water emulsions: Droplet size, rheological behavior, zeta-potential, and creaming index,” *Journal of Industrial and Engineering Chemistry*, vol. 67, pp. 123-131, 2018. Available: 10.1016/j.jiec.2018.06.022.

[35] E. Martins, D. Renard, Z. Adiwijaya, E. Karaoglan and D. Poncelet, “Oil encapsulation in core–shell alginate capsules by inverse gelation. I: dripping methodology,” *Journal of Microencapsulation*, vol. 34, no. 1, pp. 82-90, 2017. Available: 10.1080/02652048.2017.1284278.

[36] N. Tomić et al., “Image analysis and the finite element method in the characterization of the influence of porosity parameters on the mechanical properties of porous EVA/PMMA polymer blends,” *Mechanics of Materials*, vol. 129, pp. 1-14, 2019. Available: 10.1016/j.mechmat.2018.10.008.

[37] I. Hong, S. Kim and S. Lee, "Effects of HLB value on oil-in-water emulsions: Droplet size, rheological behavior, zeta-potential, and creaming index," *Journal of Industrial and Engineering Chemistry*, vol. 67, pp. 123-131, 2018. Available: 10.1016/j.jiec.2018.06.022.

[38] C. Ezeofor, "Effect of Change in Hydrophilic-Lipophilic Balance (HLB) on the State of Stable Invert Emulsion Drilling Fluid," M.S. thesis, Dept. of Chem. & Petr. Eng., Univ. of Calgary, Calgary, 2015

[39] Q. Ge, L. Ding, T. Wu, G. Xu, F. Yang and M. Xiang, "Effect of surfactant on morphology and pore size of polysulfone membrane," Journal of Polymer Research, vol. 25, no. 1, 2017. Available: 10.1007/s10965-017-1410-5.

[40] E. Ruiz-Silva, M. Rodríguez-Ortega, L. Rosales-Rivera, F. Moscoso-Sánchez, D. Rodrigue and R. González-Núñez, "Rotational Molding of Poly(Lactic Acid)/Polyethylene Blends: Effects of the Mixing Strategy on the Physical and Mechanical Properties," *Polymers*, vol. 13, no. 2, p. 217, 2021. Available: 10.3390/polym13020217.

[41] R. Shaker and D. Rodrigue, "Rotomolding of Thermoplastic Elastomers Based on Low-Density Polyethylene and Recycled Natural Rubber," *Applied Sciences*, vol. 9, no. 24, p. 5430, 2019. Available: 10.3390/app9245430.

[42] L. Utracki, *Polymer Alloys and Blends*. Munich: Hanser, 1990.

[43] J. Wefer, "Impact resistant polyethylene terephthalate/polycarbonate blends," United States Patent 4,780,506, Oct. 25, 1988.

[44] Q. Zhang, Z. Yu, X. Xie and Y. Mai, "Crystallization and impact energy of polypropylene/CaCO3 nanocomposites with nonionic modifier," *Polymer*, vol. 45, no. 17, pp. 5985-5994, 2004. Available: 10.1016/j.polymer.2004.06.044.

[45] A. Shamsuri and S. Md. Jamil, "Compatibilization Effect of Ionic Liquid-Based Surfactants on Physicochemical Properties of PBS/Rice Starch Blends: An Initial Study," *Materials*, vol. 13, no. 8, p. 1885, 2020. Available: 10.3390/ma13081885.

[46] A. Sudari, A. Shamsuri, E. Zainudin and P. Tahir, “Exploration on compatibilizing effect of nonionic, anionic, and cationic surfactants on mechanical, morphological, and chemical properties of high-density polyethylene/low-density polyethylene/cellulose biocomposites,” *Journal of Thermoplastic Composite Materials*, vol. 30, no. 6, pp. 855-884, 2015. Available: 10.1177/0892705715614064.

Chapter 5. Conclusions and Future Work

5.1 Conclusions

Rotomolded $HDPE$-$PA11$ physical blends were dry-mixed and extrusion-mixed with non-ionic surfactants, Tween 20 and Span 85. The optimum peak internal air temperature, $PIAT$ for the system was determined to be 235 °C, just prior to the onset of thermo-oxidative degradation. Zero-shear viscosities were shown to decrease with increasing Tween 20 concentrations for both $HDPE$ and $PA11$, therefore improving the melt-flow during extrusion and rotomolding processes. A downward trend was observed for porosities of both dry-mixed 50/50 and 75/25 blend ratios with extrusion-mixed samples resulting in even lower porosities compared to uncoated dry-mixed blends. Dry-mixed blends showed a drastic increase in impact strengths with an increase in Tween 20 concentration and a significant decrease in flexural strength, whereas the inverse was true for extrusion-mixed samples. Lastly, polymer migration was evident in 50/50 blends as the concentration of Tween 20 increased whereas no discernable trend was observed for 75/25 blends. Moreover, Tween 20 deteriorated the phase morphology of extrusion-mixed blends as evidenced by an increase in voidage for otherwise homogeneous morphologies.

5.2 Future Work

The results presented in this thesis have demonstrated that different combinations of non-ionic surfactant concentrations and mixing strategies can drastically influence the mechano-chemical and tensile properties of $HDPE$-$PA11$ blends. Therefore, it is highly likely that the variables investigated herein can be

manipulated to produce rotomolded plastic fuel tanks that meet or exceed the industry standard for barrier properties. To that end, the following avenues are worth exploring further:

1. The resultant properties of surfactant-compatibilized blends discussed herein have been attributed to the surface-active effects of Tween 20 on the constituent components of the polymer blend. These results however may be better explained due to the plasticization of $HDPE$ and $PA11$ in the presence of non-ionic surfactants in the system. Further investigation of the effects of different concentrations of Span 85 on $HDPE$ and $PA11$ is required to observe trends which can enable us to make meaningful conclusions in that regard.
2. Investigating and characterising penetrant (i.e. fuel) tortuous diffusivity pathways and barrier properties of non-ionic surfactant compatibilized $HDPE$-$PA11$ blends for plastic fuel tank applications.
3. Exploring the potential of using the hydrophilic-lipophilic balance value of surfactants as a predictive index for polymer migration in thermodynamically immiscible polymer blends.
4. Evaluating the behaviour of cross-linked polyethylene in scenarios similar to those investigated in this thesis owing to both the industry-wide preference and prevalence of using cross-linked polyethylene in rotomolded blends and the potential to achieve favourable tensile properties in dry-mixed rotomolded physical blends alone.